X-721-65-473

55348

NIKE TOMAHAWK NOSE OPTIMIZATION STUDIES

BY
EDWARD E. MAYO
GEORGE A. WEISSKOPF
CARL I. HUTTON, JR.

NOVEMBER 1965

NASA — GODDARD SPACE FLIGHT CENTER
GREENBELT, MARYLAND

CONTENTS

OPTIONAL FORM NO. 10
MAY 1962 EDITION
GSA GEN. REG. NO. 27
5010-107

UNITED STATES GOVERNMENT

Memorandum

TO : Flight Performance Section Files **DATE:** 27 August 1965

FROM : Mr. George A. Weisskopf
Flight Performance Section

SUBJECT: NOSE OPTIMIZATION STUDY, PART I - COMPARATIVE PERFORMANCE OF TANGENT OGIVE AND CONICAL NOSES

REFERENCE: (a) A Summary of the Supersonic Pressure Drag of Bodies of Revolution, by Deane N. Morris, Journal of the Aerospace Sciences - July 1961
(b) GD/FW Aerospace Handbook, (Fig. III.B.10-6 and III.B.10-7), Edited by R. C. Frost, General Dynamics/Fort Worth
(c) Memo of 15 March 1965, Mr. E. E. Mayo to Flight Performance Section Files, Subject: Nike-Tomahawk Particle Trajectory

Introduction:

A study is currently underway to compare sounding rocket nose shapes with reference to their effects on altitude performance, overall vehicle stability, and bending moments about the payload-rocket interface. The noses being investigated are tangent ogive and conical noses of fineness ratios 3, 5, and 7. It is hoped that the results of the study will enable an experimenter to choose on the basis of performance, stability, and bending moments the optimum nose shape for his payload-launch vehicle combination.

It is the object of this memorandum to present the progress of the study to date, and document the results of the first phase, the comparison of selected nose shapes on the basis of performance.

Performance Comparison of Tangent Ogive and Conical Noses

The sole criterion used in the performance comparison is the apogee altitude achieved when employing each of the given nose shapes. The apogee comparison is obtained through the use of an existing particle trajectory program for the Nike-Tomahawk vehicle, (Reference c). This is done by modifying the drag tables of the trajectory program according to the nose cone being tested.

The drag table in the initial program is for the Tomahawk vehicle with a fineness ratio (FR_N) of 3 tangent ogive nose. A plot of nose drag coefficient versus Mach number for each nose cone under study was obtained by the method described in the following section, and is presented herein, (Graph I). The nose drag coefficient, so obtained for the $FR_N = 3$ tangent ogive was then subtracted from the initial program table of Tomahawk plus $FR_N = 3$ tangent ogive. The remainder of this subtraction was the vehicle drag (coasting and thrusting) for the Tomahawk alone, that is, for the Tomahawk without any nose cone drag. To this basic vehicle drag the drags for each of the nose cones were added in turn thus yielding a set of drag coefficient tables, (Tables I and II). These tables were then employed in the particle trajectory program to give the desired apogee comparison.

Evaluation of Individual Nose Drag Coefficients

The evaluation of nose drag coefficients is broken down into a consideration of pressure drag and skin friction drag. It is initially considered that the pressure drag is the predominant factor, and that any significant nose performance advantages will show up by using the different pressure drags only.

Skin friction drag is a function of wetted surface area. In this performance comparison it is reasonable to assume that in going from one nose shape to another an experimenter would not substantially increase or decrease the total wetted surface area of the payload covering (nose cone and cylindrical afterbody). The reason for this assumption is that in using the smaller fineness ratio nose cones more cylindrical afterbody length is required to cover a given volume payload. Therefore, any change in skin friction drag in going from one nose shape to another will be very small in comparison to the pressure drag change. On this basis then the skin friction drag has been neglected in this initial performance comparison.

The pressure drag coefficient for each nose shape was computed on the basis of references (a and b) for the Mach number range ($M_\infty = 1.25$ to $M_\infty = 10.00$). The method of computation is simple and involves only reading values from two (2) graphs and division by a constant conversion factor. The results of this computation have been plotted, and appear in Graph I.

Limiting Cases

In addition to the three tangent ogive and three conical noses compared, two limiting conditions were also investigated. The first of these conditions is the case of a hemispherical nose (tangent ogive $FR_N = .5$) representing a maximum drag case. The pressure drag coefficient for this nose is plotted in Graph II, and the drag coefficient tables for

this case are given in Table III. The second condition is that of a zero drag nose representing a minimum drag case. These cases have been included in order to determine the performance of the FR_N = 3, 5, and 7 cones and ogives relative to these limiting conditions.

Results and Conclusions

The results of the first phase of the nose optimization study, together with the aforementioned limiting cases, are presented in Table IV. The differences in altitude between tangent ogive and conical noses of the same fineness ratios is only about 1 mile in 200 (1/2%). The maximum difference in apogee altitude is only 12 miles in 200 (6%), this being between an FR_N = 3 ogive and FR_N = 7 cone.

All the conical and tangent ogive noses yielded apogee altitudes below but within 16 miles of the optimum (214.26 miles) given by the zero drag nose. The apogee altitude of the hemisphere case turned out to be surprisingly low (92.56 miles). It is possible that this low value may be due to an error in calculation, but so far no such error has been found.

Since all the noses group themselves close to the maximum zero dray nose in apogee altitude, it may be desirable to recompute the drag tables to include skin friction drag. This may be expected to lower the apogee altitude of each nose slightly, but probably will not change the relative differences in apogee altitude between the various noses.

The close grouping in altitude performance, particularly between tangent ogive and conical noses of the same fineness ratios, would seem to indicate that this will not be a major factor in the selection of a nose shape. Probably the nose shape effects on stability will be more important, and this is the area which is now being investigated.

George A. Weisskopf

Enclosures

cc: Mr. K. R. Medrow
Miss E. C. Pressly
Mr. E. E. Mayo
Mr. G. R. Barlow
Mr. J. T. Lawrence
Mr. J. S. Barrowman

GAW:skd

SYMBOLS AND DEFINITIONS*

$C_{D_{PN}}$ = Nose Pressure Drag Coefficient

M_{∞} = Free-Stream Mach Number

C_{D_T} = Total Vehicle Thrusting Drag Coefficient

C_{D_C} = Total Vehicle Coasting Drag Coefficient

R_{ap} = Vehicle Apogee Altitude

FR_N = Nose Fineness Ratio

*Aerodynamic reference area = 0.4418 sq. ft.

TABLE I

Thrusting Drag Coefficients for Tomahawk and Indicated Nose Cone

	Without Nose Cone	Ogives			Cones		
		$FR_N=3$	$FR_N=5$	$FR_N=7$	$FR_N=3$	$FR_N=5$	$FR_N=7$
M_∞	C_{D_T}	C_{D_T}	C_{D_T}	C_{D_T}	C_{D_T}	C_{D_T}	C_{D_T}
1.25	.8420	.9550	.8850	.8642	.9728	.8995	.8746
1.95	.6985	.8000	.7390	.7200	.7960	.7412	.7233
2.00	.6420	.7250	.6642	.6453	.7203	.6663	.6484
2.20	.5761	.6750	.6157	.5972	.6679	.6165	.5995
2.45	.5287	.6250	.5674	.5495	.6160	.5668	.5510
2.70	.4911	.5850	.5292	.5117	.5744	.5281	.5124
2.75	.4765	.5700	.5145	.4970	.5590	.5132	.4976
2.90	.4578	.5500	.4954	.4781	.5383	.4936	.4786
3.00	.4487	.5400	.4861	.4689	.5280	.4840	.4691
3.10	.4346	.5250	.4717	.4546	.5129	.4695	.4547
3.35	.4116	.5000	.4481	.4315	.4873	.4453	.4312
3.50	.4027	.4900	.4387	.4225	.4770	.4360	.4219
3.75	.3845	.4700	.4202	.4041	.4570	.4169	.4032
4.10	.3665	.4500	.4015	.3859	.4370	.3977	.3846
4.40	.3579	.4400	.3924	.3770	.4273	.3882	.3755
4.90	.3348	.4150	.3684	.3535	.4025	.3637	.3519
5.85	.3076	.3850	.3399	.3256	.3731	.3346	.3234
9.00	.2185	.2900	.2500	.2340	.2798	.2425	.2319

TABLE II

Coasting Drag Coefficients for Tomahawk and Indicated Nose Cone

	Without Nose Cone	Ogives			Cones		
		$FR_N=3$	$FR_N=5$	$FR_N=7$	$FR_N=3$	$FR_N=5$	$FR_N=7$
M_∞	C_{D_C}	C_{D_C}	C_{D_C}	C_{D_C}	C_{D_C}	C_{D_C}	C_{D_C}
1.25	1.0520	1.1650	1.0951	1.0746	1.1828	1.1095	1.0846
1.60	.8938	1.0000	.9356	.9158	1.0020	.9417	.9210
1.90	.7978	.9000	.8383	.8194	.8965	.8412	.8229
2.20	.7013	.8000	.7409	.7224	.7931	.7416	.7246
2.50	.6343	.7300	.6730	.6551	.7206	.6725	.6564
2.90	.5578	.6500	.5954	.5780	.6383	.5936	.5785
3.25	.5107	.6000	.5475	.5307	.5874	.5450	.5304
3.50	.4777	.5650	.5140	.4975	.5520	.5110	.4969
3.75	.4545	.5400	.4903	.4740	.5297	.4869	.4732
4.00	.4360	.5200	.4712	.4554	.5070	.4683	.4558
4.30	.4175	.5000	.4522	.4366	.4872	.4480	.4372
4.75	.3915	.4720	.4254	.4104	.4597	.4208	.4087
5.25	.3661	.4450	.3991	.3846	.4329	.3943	.3825
6.00	.3380	.4150	.3700	.3560	.4032	.3648	.3536
7.00	.3052	.3800	.3359	.3225	.3688	.3307	.3199
9.00	.2435	.3150	.2725	.2595	.3048	.2675	.2569
999.00	.2435	.3150	.2725	.2595	.3048	.2675	.2569

TABLE III

Thrusting and Coasting Drag Coefficients for the Tomahawk with Hemispherical Nose

M_∞	C_{D_T}
1.25	1.4120
1.95	1.4565
2.00	1.3840
2.20	1.3561
2.45	1.3257
2.70	1.3011
2.75	1.2935
2.90	1.2758
3.00	1.2707
3.10	1.2596
3.35	1.2446
3.50	1.2387
3.75	1.2245
4.10	1.2115
4.40	1.2049
4.90	1.1888
5.85	1.1716
9.00	1.0965

M_∞	C_{D_C}
1.25	1.6220
1.60	1.5888
1.90	1.5448
2.20	1.4813
2.50	1.4343
2.90	1.3758
3.25	1.3407
3.50	1.3137
3.75	1.2945
4.00	1.2810
4.30	1.2655
4.75	1.2415
5.25	1.2261
6.00	1.2050
7.00	1.1772
9.00	1.1215
999.00	1.1215

TABLE IV

Altitude Performance:

Nose Configuration	Apogee Altitude (R_{ap})	
	Statute Miles	Feet
Ogive, FR_N=3	198.02847	1,044,843.2
Ogive, FR_N=5	207.44315	1,094,517.2
Ogive, FR_N=7	210.57304	1,111,031.2
Cone, FR_N=3	199.93661	1,054,911.0
Cone, FR_N=5	208.17190	1,098,362.2
Cone, FR_N=7	210.74570	1,111,942.2

Limiting Cases:

Nose Configuration	Apogee Altitude (R_{ap})	
	Statute Miles	Feet
Zero Drag Nose	214.26512	1,130,511.5
Hemisphere (Ogive FR_N=.5)	92.568841	488,414.25

Graph - I

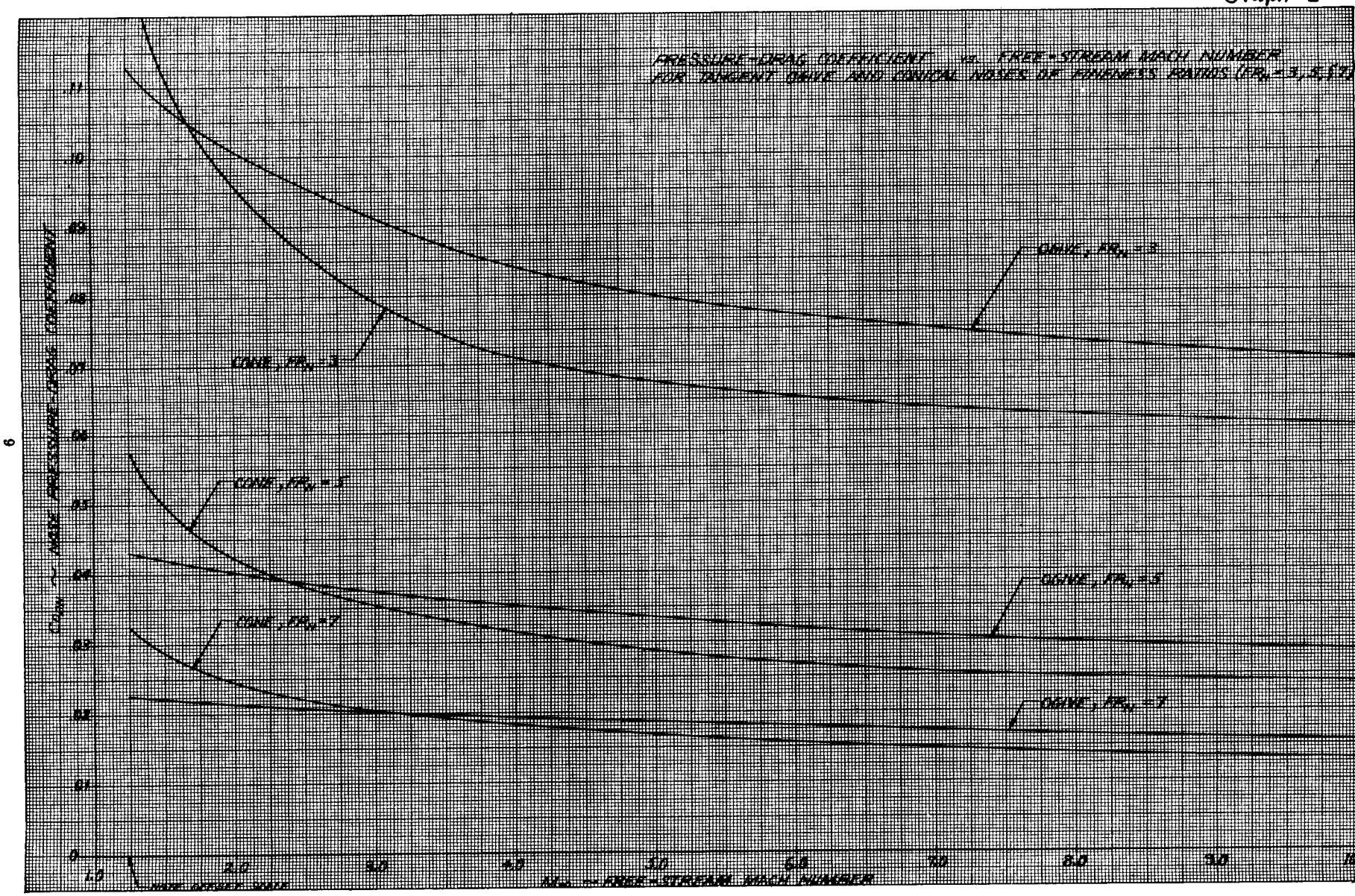
PRESSURE-DRAG COEFFICIENT vs. FREE-STREAM MACH NUMBER
FOR TANGENT OGIVE AND CONICAL NOSES OF FINENESS RATIOS (FR_N = 3, 5, & 7)
$C_{D_{WP}}$ - WAVE PRESSURE-DRAG COEFFICIENT
M_∞ - FREE-STREAM MACH NUMBER
WAVE ONSET POINT
CONE, FR_N = 3
CONE, FR_N = 5
CONE, FR_N = 7
OGIVE, FR_N = 3
OGIVE, FR_N = 5
OGIVE, FR_N = 7
1.1
1.0
.9
.8
.7
.6
.5
.4
.3
.2
.1
0
1.0
2.0
3.0
4.0
5.0
6.0
7.0
8.0

Graph-II

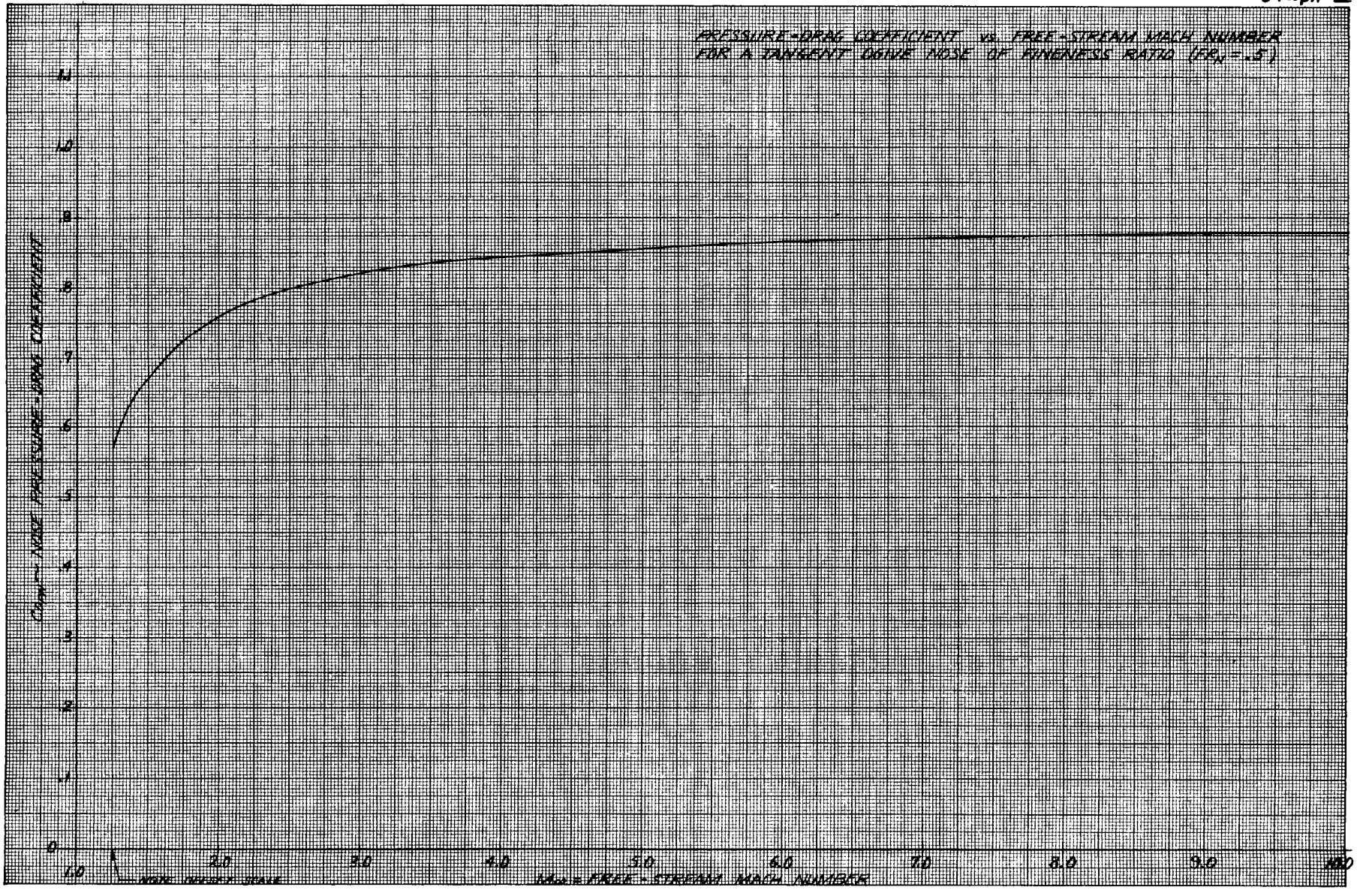
PRESSURE-DRAG COEFFICIENT vs. FREE-STREAM MACH NUMBER
FOR A TANGENT OGIVE NOSE OF FINENESS RATIO (f_{ON} = 5)
$C_{D_{WAVE}}$ = WAVE PRESSURE-DRAG COEFFICIENT
11
10
9
8
7
6
5
4
3
2
1
0
1.0
2.0
3.0
4.0
5.0
6.0
7.0
8.0
9.0
10
M_∞ = FREE-STREAM MACH NUMBER

OPTIONAL FORM NO. 10
MAY 1962 EDITION
GSA GEN. REG. NO. 27
5010-107

UNITED STATES GOVERNMENT

Memorandum

TO : Flight Performance Section Files DATE: 11 October 1965

FROM : Mr. Edward E. Mayo
Flight Performance Section

SUBJECT: NOSE OPTIMIZATION STUDY, PART II - STABILITY AND PAYLOAD-ROCKET INTERFACE BENDING MOMENTS, CASE I

REFERENCE:
(a) Memo of 27 August 1965, Mr. G. A. Weisskopf to Flight Performance Section Files, Subject: Nose Optimization Study, Part I - Comparative Performance of Tangent Ogive and Conical Noses
(b) Memo of 29 June 1965, Mr. E. E. Mayo to Flight Performance Section Files, Subject: Effect of Payload Weight on the Tomahawk Mass, Static Margin, Static Stability, and Natural Frequency Characteristics
(c) Syverston, Clarence A. and Dennis, David H.: A Second-Order Shock-Expansion Method Applicable to Bodies of Revolution Near Zero Lift, NACA Report 1328, 1957

INTRODUCTION

A study is currently underway to investigate the feasibility of optimizing sounding rocket nose shapes. Ultimately, it is hoped to arrive at design curves such that an experimenter may choose the optimum nose shape based on his particular payload weight, volume, and packaging requirements. To achieve this end, certain optimization parameters must be chosen. For this study the parameters selected were apogee altitude, vehicle stability and payload-rocket interface bending moment. The nose shapes considered herein are cones and ogives having fineness ratios of 3, 5 and 7. In order to expedite calculations, the geometry of the Tomahawk configuration shown in figure 1 is being used as a study model. A study delineating the effects of nose shape on apogee altitude has been reported in reference (a). The study presented herein examines the vehicle stability and payload-rocket interface bending moments for payload weight distribution Case I. (Constant density payload contained within payload cylindrical section, see figure 1.) A study investigating payload weight distribution Case II (constant volume and constant density payload) is now underway. It is believed that these two cases should bracket actual weight distributions; and, hence, if the same conclusions can be drawn from these cases, they should also apply for the actual distribution.

ANALYSIS

Trajectory and mass characteristics. - The pertinent trajectory characteristics, Mach number and dynamic pressure, are given in figure 2 for the extreme nose shapes (f_n = 3 ogive and f_n = 7 cone) as extracted from the runs of reference (a). The invariancy of these characteristics with nose shape allows, as will be seen later, direct comparison of changes in stability and payload-rocket interface bending moments as a function of only Mach number. The vehicle weight, center-of-gravity location and pitch moment of inertia are presented in figure 3. The vehicle without payload mass characteristics used in obtaining the values in figure 3 were obtained from reference (b).

Stability. - The stability characteristics for the various noses were determined by modifying the Tomahawk configuration (figure 1, f_n = 3 ogive) aerodynamics which are given in Table I. The fin + interference characteristics were obtained by utilizing the f_n = 3 ogive, f_a = 10 body characteristics of Table II(a). The fin + interference values are given by

$$C_{N_{\alpha}}{}_{(f+i)} = C_{N_{\alpha}} - C_{N_{\alpha}}{}_{(n+a)} \Bigg|_{\substack{f_n = 3 \text{ ogive} \\ f_a = 10}} \tag{1}$$

$$(x_{cp}/d)_{(f+i)} = \frac{C_{N_{\alpha}}(x_{cp}/d) - \left[C_{N_{\alpha}}{}_{(n+a)} \; (x_{cp}/d)_{(n+a)} \right]_{\substack{f_n = 3 \text{ ogive} \\ f_a = 10}}}{C_{N_{\alpha}}{}_{(f+i)}} \tag{2}$$

The vehicle stability characteristics were then obtained by combining the fin + interference values with the various fineness ratio nose values of Table II(a). The vehicle stability equations are

$$C_{N_{\alpha}} = C_{N_{\alpha}}{}_{(f+i)} + C_{N_{\alpha}}{}_{(n+a)} \Bigg|_{f_a = 10} \tag{3}$$

$$x_{cp}/d = \frac{C_{N_{\alpha}}{}_{(f+i)} \; (x_{cp}/d)_{(f+i)} + \left[C_{N_{\alpha}}{}_{(n+a)} \left(\frac{x_{cp}}{d} \right)_{(n+a)} \right]_{f_a = 10}}{C_{N_{\alpha}}} \tag{4}$$

The resulting stability characteristics are given in Table III and incremental static margins from the $f_n = 3$ ogive values are presented in figure 4. From figure 4, the optimum nose shape depends on the Mach number of minimum stability. For ogives (figure 4(a)) and Mach numbers greater than about 3.5, the lower fineness ratio noses yield greater stability; and at Mach numbers lower than about 3.5, the higher fineness ratio noses tend to yield greater stability. For cones (figure 4(b)) the higher fineness ratio yields greater stability; however, for Mach numbers greater than about 5, the stability is less than the basic $f_n = 3$ ogive and for Mach numbers less than about 5 the stability is greater than the basic $f_n = 3$ ogive. For the Tomahawk, the Mach number for minimum stability is about 8; hence, figure 4 indicates that the $f_n = 3$ ogive yields the largest minimum static margin.

Payload-rocket interface bending moments. - The payload-rocket interface bending moments were assumed to be composed of aerodynamic, rotational inertia and translational inertia components, i.e.,

$$\frac{m}{\alpha qsd} = \left|\frac{m}{\alpha qsd}\right|_{\substack{\text{Aerodynamic}}} + \left|\frac{m}{\alpha qsd}\right|_{\substack{\text{Rotational}\\\text{Inertia}}} - \left|\frac{m}{\alpha qsd}\right|_{\substack{\text{Translational}\\\text{Inertia}}} \tag{5}$$

which may be expressed as

$$\frac{m}{\alpha qsd} = C_{N_\alpha}{}_{(n+a)} \left|_{\substack{f_n \\ f_a = 4.4}}\right. \left(f_n + f_a - \frac{\bar{x}_{cp}}{d}\right)_{f_a = 4.4} - \frac{(I_p)_{p.i.}}{I} \quad C_{m_\alpha}$$

$$- \left(\frac{W_p}{W}\right) C_{N_\alpha} \left[f_n + f_a - (\bar{x}_{cg}/d)_p\right]_{f_a = 4.4} \tag{6}$$

where the $f_a = 4.4$ aerodynamic characteristics are given in Table II(b). The resulting nondimenionalized bending moments are summarized in Table IV and the incremental nondimenionalized bending moments from the $f_n = 3$ ogive values are shown in figure 5. From figure 5, an increase in fineness ratio results in increased payload-rocket interface bending moments for both ogive and conical noses with severe bending moments resulting from the higher fineness ratio ogives. It is also seen that the bending moments for a cone are not as severe as those for an ogive of the same fineness ratio.

SUMMARY

In summary, the procedures described herein will allow an intelligent choice of the optimum nose shape from stability and payload-rocket interface bending moment considerations. For the Tomahawk vehicle, the optimum nose from stability considerations is the 3:1 ogive; however, from bending moment considerations, the optimum nose is the 3:1 cone. The choice between these would, of course, depend upon the minimum static margin, packaging requirements and structural integrity of the payload-rocket interface of the flight configuration under consideration.

The discussions in this memo are for the flight configuration shown in figure 1 and payload weight distribution Case I. Studies parallel to those presented herein are underway for the same flight configuration and payload weight distribution Case II.

Edward E. Mayo

Edward E. Mayo

Enclosures:
(1) Symbols
(2) Tables (4)
(3) Figures (5)

cc: Mr. K. R. Medrow
Mr. G. E. MacVeigh
Mr. E. F. Sorgnit
Mr. E. E. Bissell
Miss E. C. Pressly
Mr. N. E. Peterson, Jr.
Mr. J. H. Lane
Mr. J. T. Lawrence, Jr.
Mr. J. S. Barrowman
Mr. H. L. Galloway, Jr.
Mr. G. R. Barlow

EEM: skd

SYMBOLS

C_{N_α}	normal force coefficient curve slope at $\alpha = 0$, per radian
d	reference diameter, d = 0.75 ft.
f	fineness ratio
I	pitch inertia
M	free-stream Mach number
m	bending moment at payload-rocket interface
q	free-stream dynamic pressure
S	reference area, $S = \frac{\pi d^2}{4}$
S.M.	static margin, minus for positive stability
t	time, sec.
x	longitudinal distance measured forward of base
$\bar{x}$	longitudinal distance measured aft of nose apex
W	weight
α	angle of attack, radians

SUBSCRIPTS

a	cylindrical afterbody
cg	center-of-gravity location
cp	center-of-pressure location
n	nose
p	payload
p.i.	payload interface

TABLE I. - Aerodynamic Characteristics of Tomahawk Sounding Rocket.*
f_n = 3 ogive.

Mach	C_{N_α}	x_{cp}, feet
3.00	14.10	4.002
4.24	11.14	5.015
5.05	10.20	5.530
6.28	9.37	6.170

*Reference (b)

TABLE II. - Aerodynamic Characteristics of Tangent Ogive-Cylinder and Cone-Cylinder Configurations.*

(a) $f_a = 10$

$C_{N_{\alpha_{(n+a)}}}$

M \ f_n	Ogives			Cones		
	3	5	7	3	5	7
3.00	3.32	3.06	2.85	3.37	3.01	2.84
4.24	3.34	3.18	3.11	3.45	3.21	2.85
5.05	3.38	3.29	3.02	3.63	3.26	3.06
6.28	2.90	3.31	3.24	3.37	3.22	2.99

$(\bar{x}_{cp}/d)_{(n+a)}$

M \ f_n	Ogives			Cones		
	3	5	7	3	5	7
3.00	2.60	3.75	4.55	3.51	4.88	6.32
4.24	3.12	4.09	5.16	3.82	5.39	6.39
5.05	3.60	4.06	5.23	3.82	5.25	6.55
6.28	3.05	4.32	5.58	3.77	5.32	6.74

*Experimental data of reference (c).

TABLE II. - Concluded.

(b) $f_a = 40/9 = 4.44$

$(C_{N_\alpha})_{(n+a)}$

M \ f_n	Ogives			Cones		
	3	5	7	3	5	7
3.00	3.29	2.99	2.84	3.21	2.91	2.75
4.24	3.20	3.02	3.00	3.18	2.90	2.80
5.05	3.09	3.08	2.99	3.20	2.90	2.80
6.28	2.67	2.90	2.91	2.99	2.80	2.63

$\left.\frac{\bar{x}_{cp}}{d}\right|_{(n+a)}$

M \ f_n	Ogives			Cones		
	3	5	7	3	5	7
3.00	2.45	3.35	4.30	3.01	4.45	5.70
4.24	2.55	3.60	4.75	3.27	4.70	6.00
5.05	2.90	3.75	4.90	3.30	4.65	5.99
6.28	2.50	3.70	4.85	3.25	4.65	5.99

TABLE III. - Aerodynamic Characteristics of Tomahawk Sounding Rocket with Various Fineness Ratio Noses.

(a) Ogives

M	t_s, sec	C_{N_α}	S.M. Calibers	Δ S.M.* Calibers
$f_n = 3$				
3	2.2	14.10	-4.44	0
4.24	3.85	11.14	-3.24	0
5.05	4.83	10.20	-2.68	0
6.28	6.27	9.37	-1.99	0
$f_n = 5$				
3	2.2	13.84	-4.54	-0.10
4.24	3.85	10.98	-3.13	+0.11
5.05	4.83	10.11	-2.28	+0.40
6.28	6.27	9.78	-1.25	+0.74
$f_n = 7$				
3	2.2	13.63	-4.53	-0.09
4.24	3.85	10.91	-2.95	+0.29
5.05	4.83	9.84	-2.39	+0.29
6.28	6.27	9.71	-1.09	+0.90

*Δ S.M. = S.M.$\Big|_{f_n}$ - S.M.$\Big|_{f_n = 3 \text{ ogive}}$. + indicates decreased stability

TABLE III. - Concluded

(b) Cones

M	t, sec	$C_{N_{\alpha}}$	S.M. Calibers	Δ S.M.* Calibers
		$f_n = 3$		
3	2.2	14.15	-4.61	-0.17
4.24	3.85	11.25	-3.32	-0.08
5.05	4.83	10.45	-2.47	+0.21
6.28	6.27	9.84	-1.68	+0.31
		$f_n = 5$		
3	2.2	13.79	-4.84	-0.40
4.24	3.85	11.01	-3.47	-0.23
5.05	4.83	10.08	-2.71	-0.03
6.28	6.27	9.69	-1.69	+0.30
		$f_n = 7$		
3	2.2	13.62	-4.92	-0.48
4.24	3.85	10.65	-3.64	-0.40
5.05	4.83	9.88	-2.74	-0.06
6.28	6.27	9.46	-1.78	+0.21

*Δ S.M. = S.M.$\Big|_{f_n}$ - S.M.$\Big|_{f_n = 3 \text{ ogive}}$. + indicates decreased stability

TABLE IV. - Payload-Rocket Interface Nondimensionalized Bending Moment, $\frac{m}{\alpha qsd}$

(a) Ogives

Mach	$m/\alpha qsd$ / t, sec	Aero.	Rotational Inertia	Translational Inertia	Total	$\frac{\Delta m^*}{\alpha qsd}$
		$f_n = 3$				
3	2.2	16.42	2.63	-6.95	12.1	0
4.24	3.85	15.65	1.45	-6.46	10.6	0
5.05	4.83	14.03	1.27	-6.59	8.7	0
6.28	6.27	13.19	.92	-7.07	7.0	0
		$f_n = 5$				
3	2.2	18.21	2.64	-6.82	14.0	1.9
4.24	3.85	17.64	1.55	-6.36	12.8	2.2
5.05	4.83	17.53	1.07	-6.53	12.1	3.4
6.28	6.27	16.65	.61	-7.38	9.9	2.9
		$f_n = 7$				
3	2.2	20.28	2.60	-6.72	16.2	4.1
4.24	3.85	20.07	1.45	-6.32	15.2	4.6
5.05	4.83	19.55	1.09	-6.36	14.3	5.6
6.28	6.27	19.18	.52	-7.33	12.4	5.4

$$* \frac{\Delta m}{\alpha qsd} = \frac{m}{\alpha qsd}\bigg|_{f_n} - \frac{m}{\alpha qsd}\bigg|_{f_n = 3 \text{ ogive}}$$

TABLE IV. - Concluded.

(b) Cones

Mach	$m/\alpha qsd$ / t, sec	Aero.	Rotational Inertia	Translational Inertia	Total	$\frac{\Delta m^*}{\alpha qsd}$
$f_n = 3$						
3	2.2	14.22	2.74	-6.97	10.0	-2.1
4.24	3.85	13.26	1.68	-6.52	8.4	-2.2
5.05	4.83	13.25	1.20	-6.75	7.7	-1.0
6.28	6.27	12.53	.82	-7.43	5.9	-1.1
$f_n = 5$						
3	2.2	14.52	2.81	-6.80	10.5	-1.6
4.24	3.85	13.75	1.72	-6.38	9.1	-1.5
5.05	4.83	13.89	1.27	-6.51	8.6	-0.1
6.28	6.27	13.41	.81	-7.31	6.9	-0.1
$f_n = 7$						
3	2.2	15.78	2.82	-6.71	11.9	-0.2
4.24	3.85	15.23	1.74	-6.17	10.8	0.2
5.05	4.83	15.26	1.26	-6.38	10.1	1.4
6.28	6.27	14.33	.84	-7.14	8.0	1.0

* $\frac{\Delta m}{\alpha qsd} = \frac{m}{\alpha qsd}\Big|_{f_n} - \frac{m}{\alpha qsd}\Big|_{f_n = 3 \text{ ogive}}$

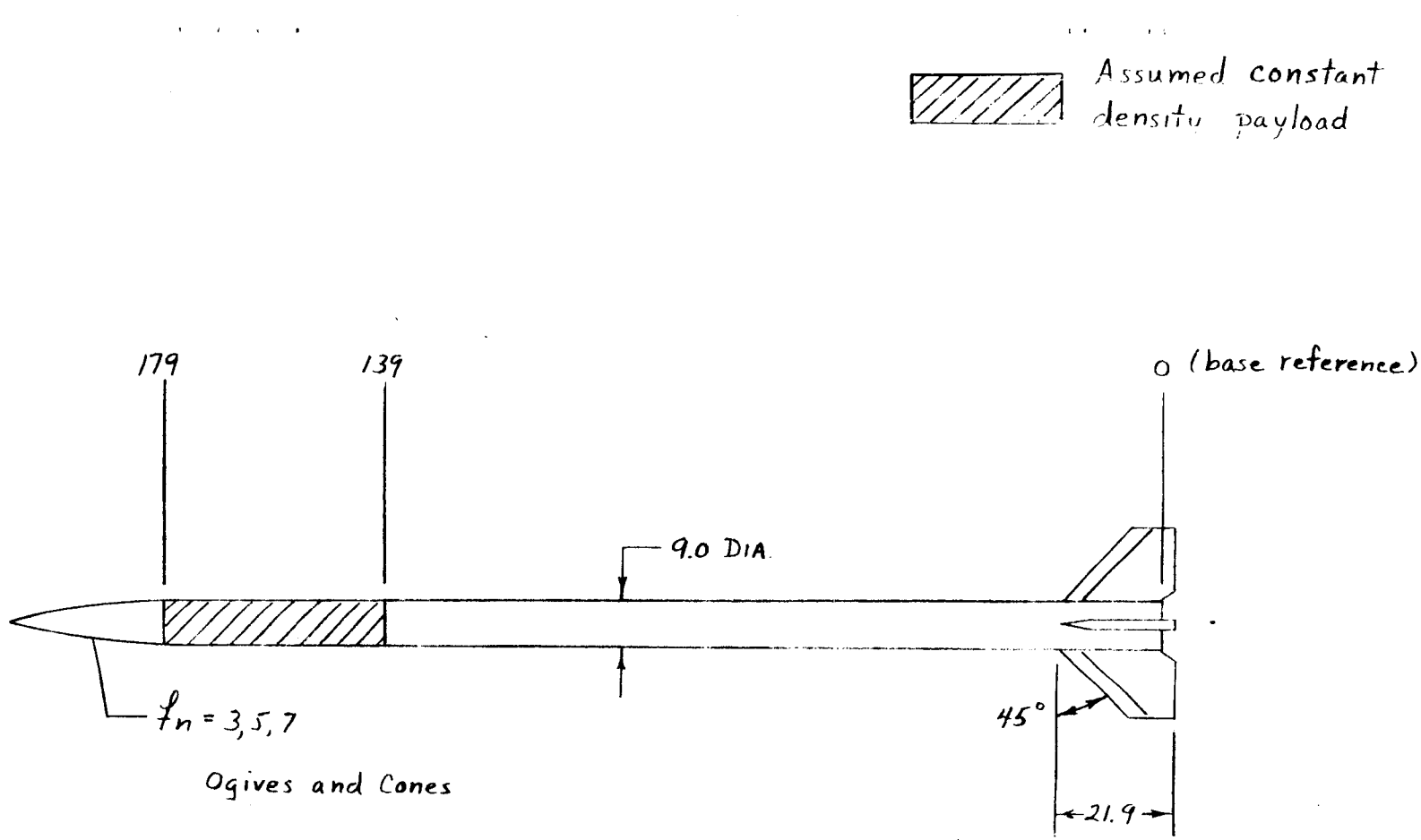

Payload weight distribution. Case I

Figure 1. - Tomahawk TE-416 sounding rocket. All dimensions are in inches.

Gross payload weight = 123 lbs.

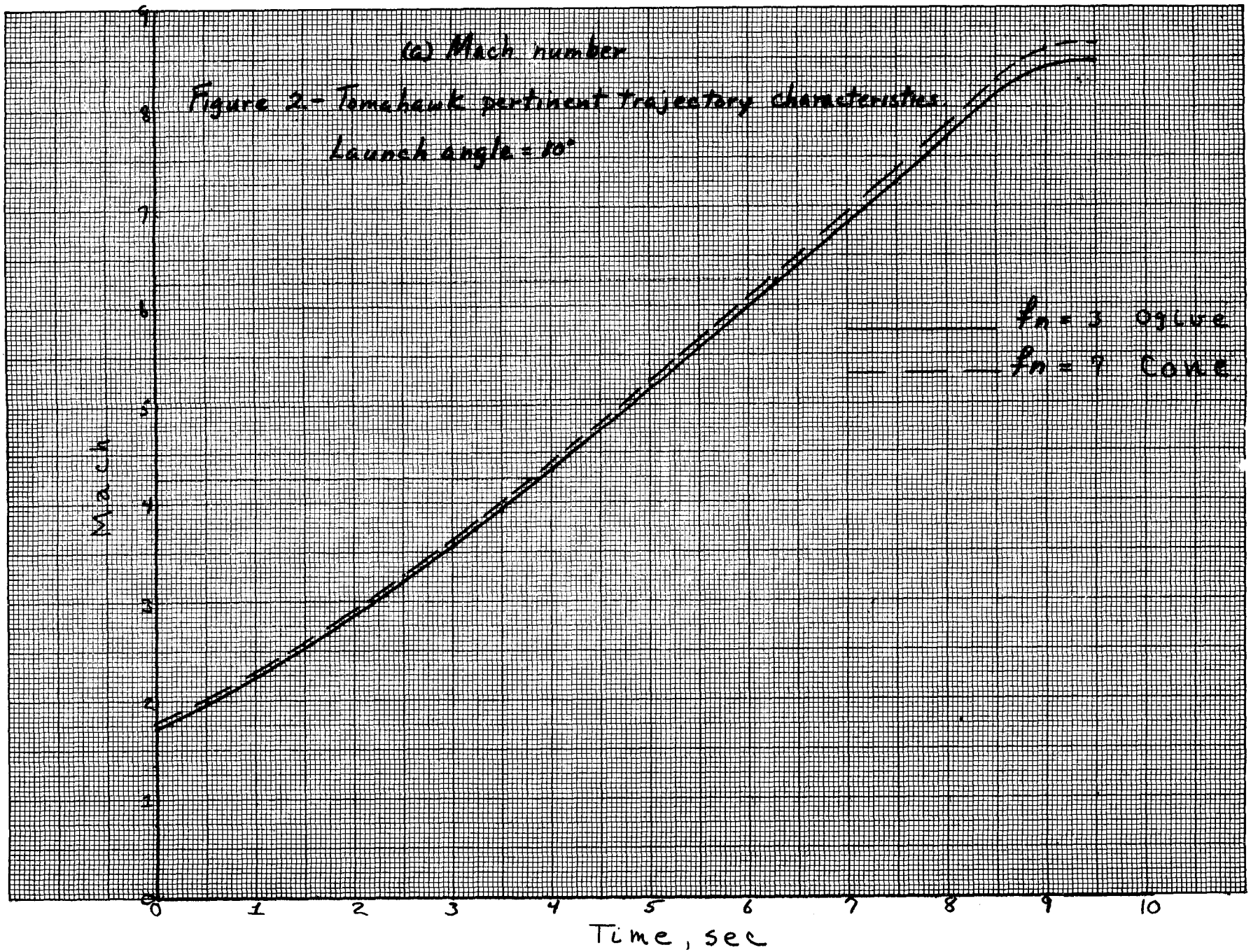

Figure 2.- Tomahawk pertinent trajectory characteristics.

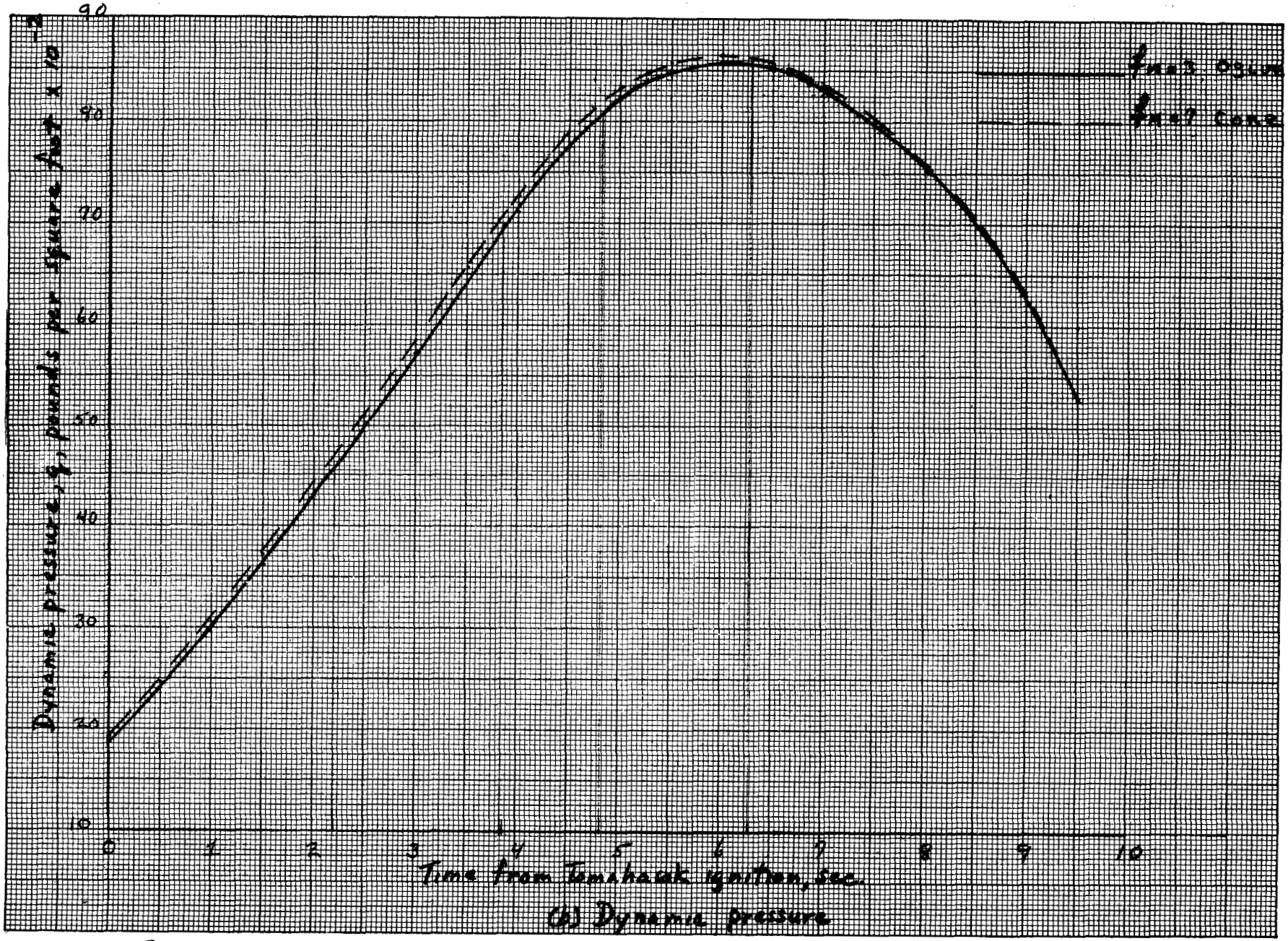

(b) Dynamic pressure.

Figure 2.- Concluded.

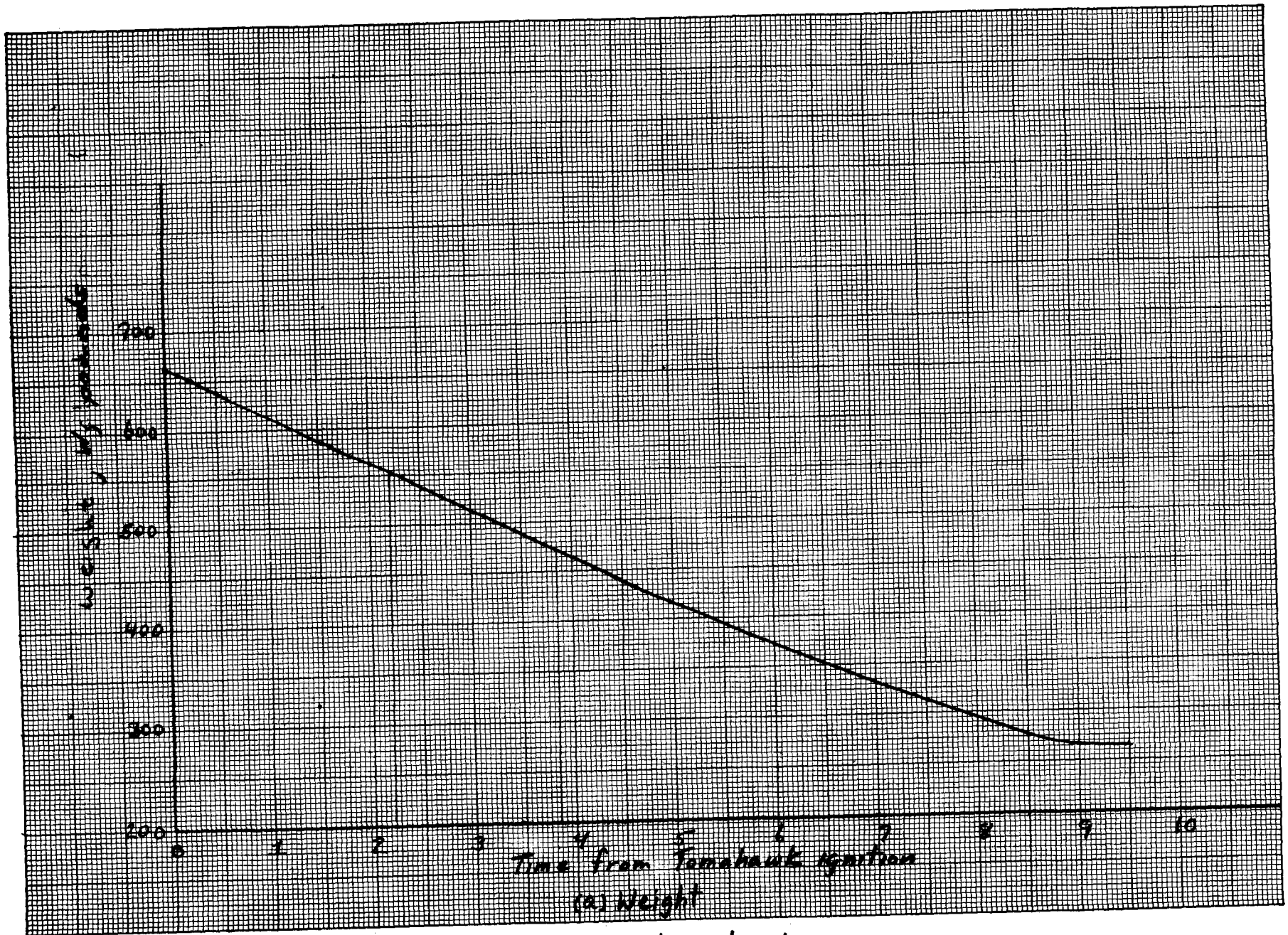

Figure 3.- Tomahawk pertinent mass characteristics.

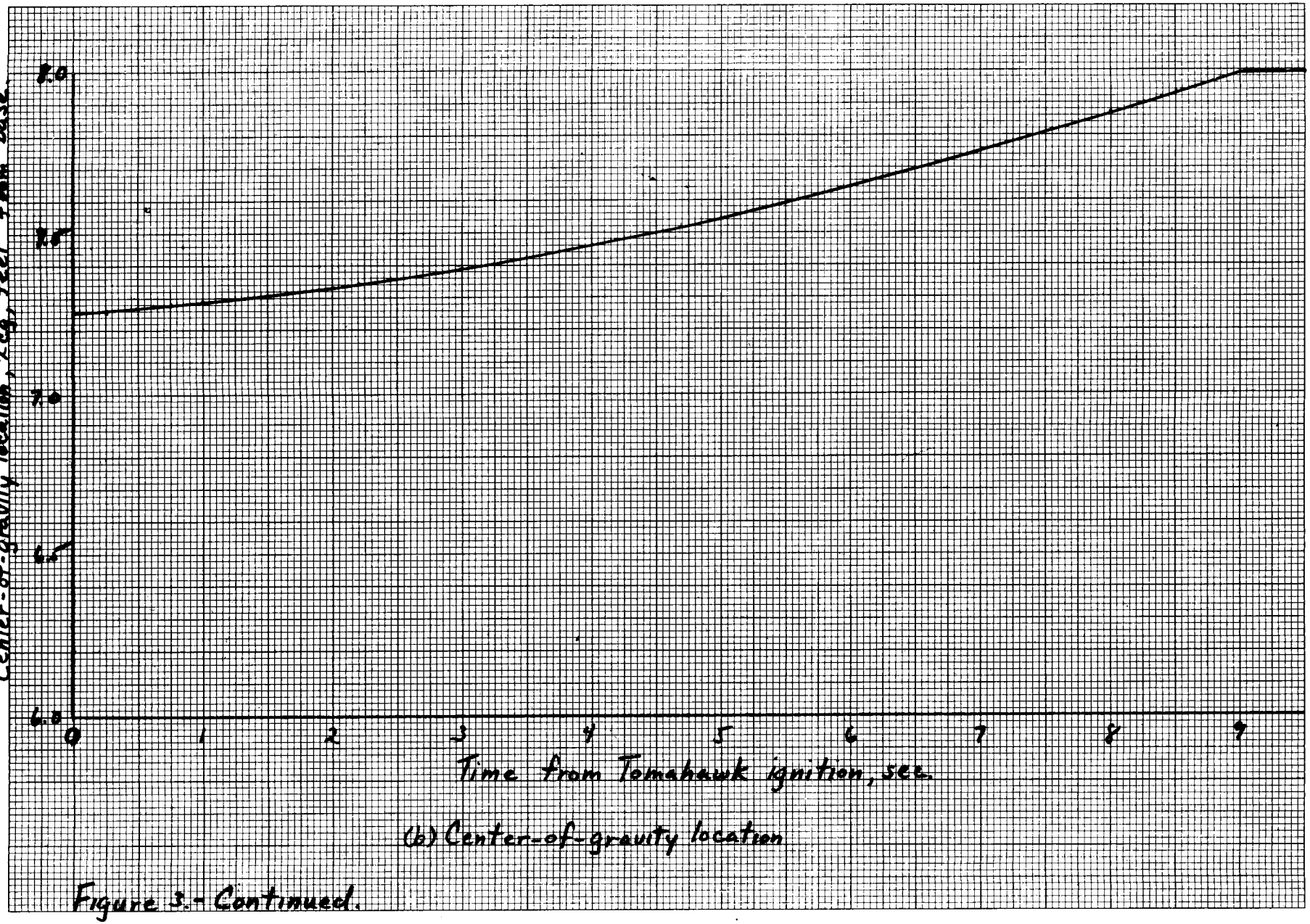

(b) Center-of-gravity location

Figure 3.- Continued.

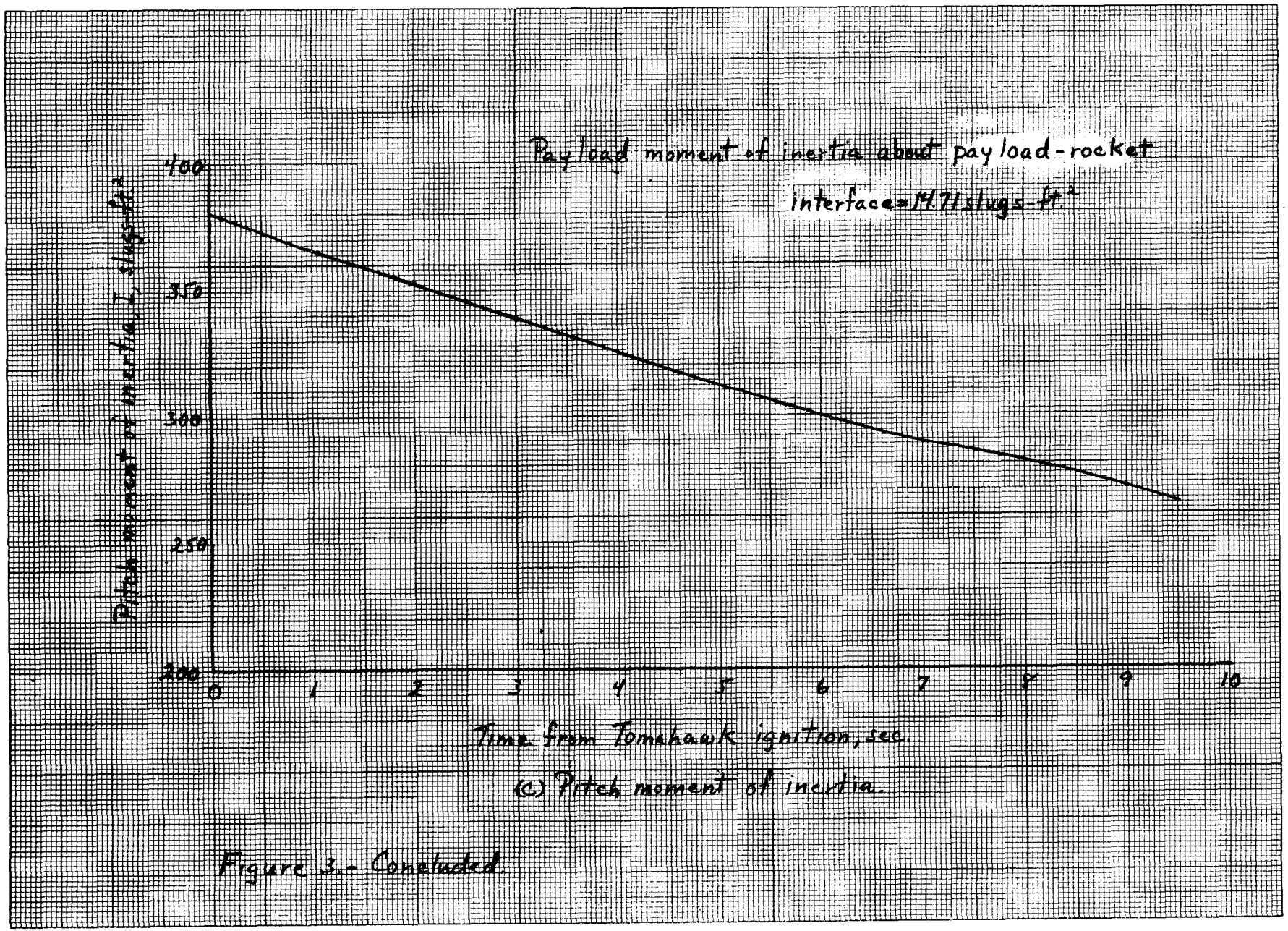

(c) Pitch moment of inertia.

Figure 3.- Concluded.

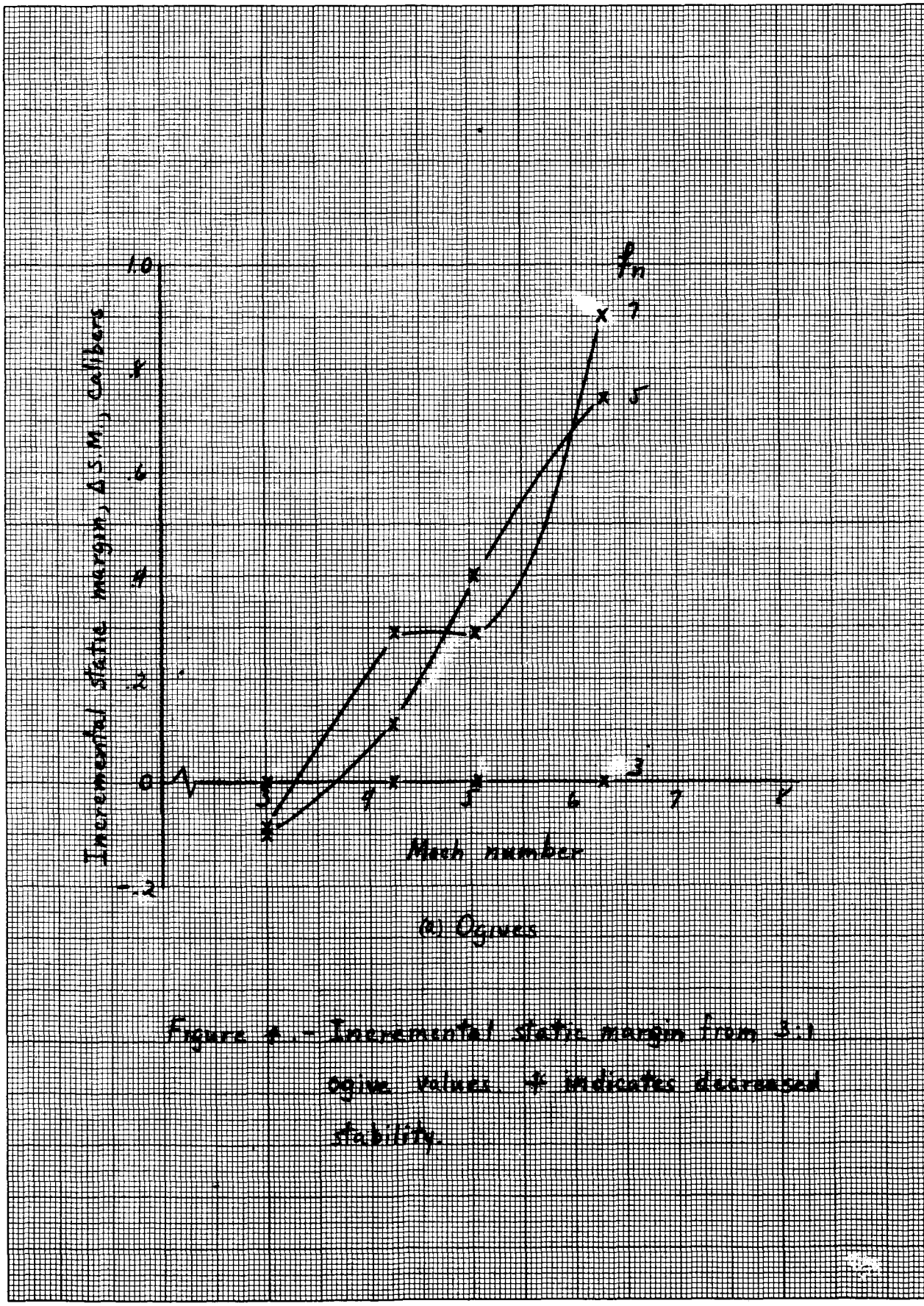

(a) Ogives

Figure 4.- Incremental static margin from 3:1 ogive values. * indicates decreased stability.

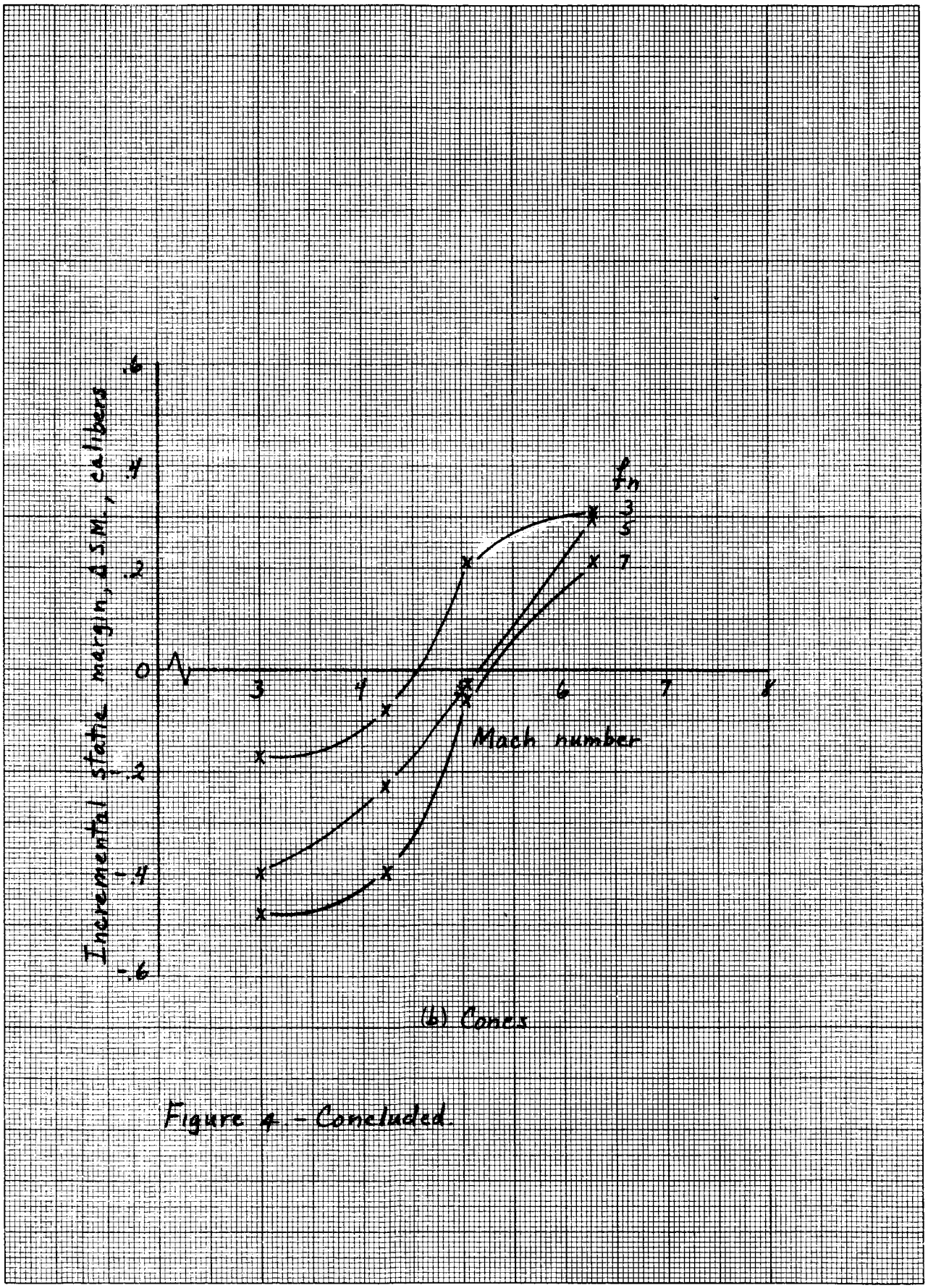

(b) Cones

Figure 4. - Concluded.

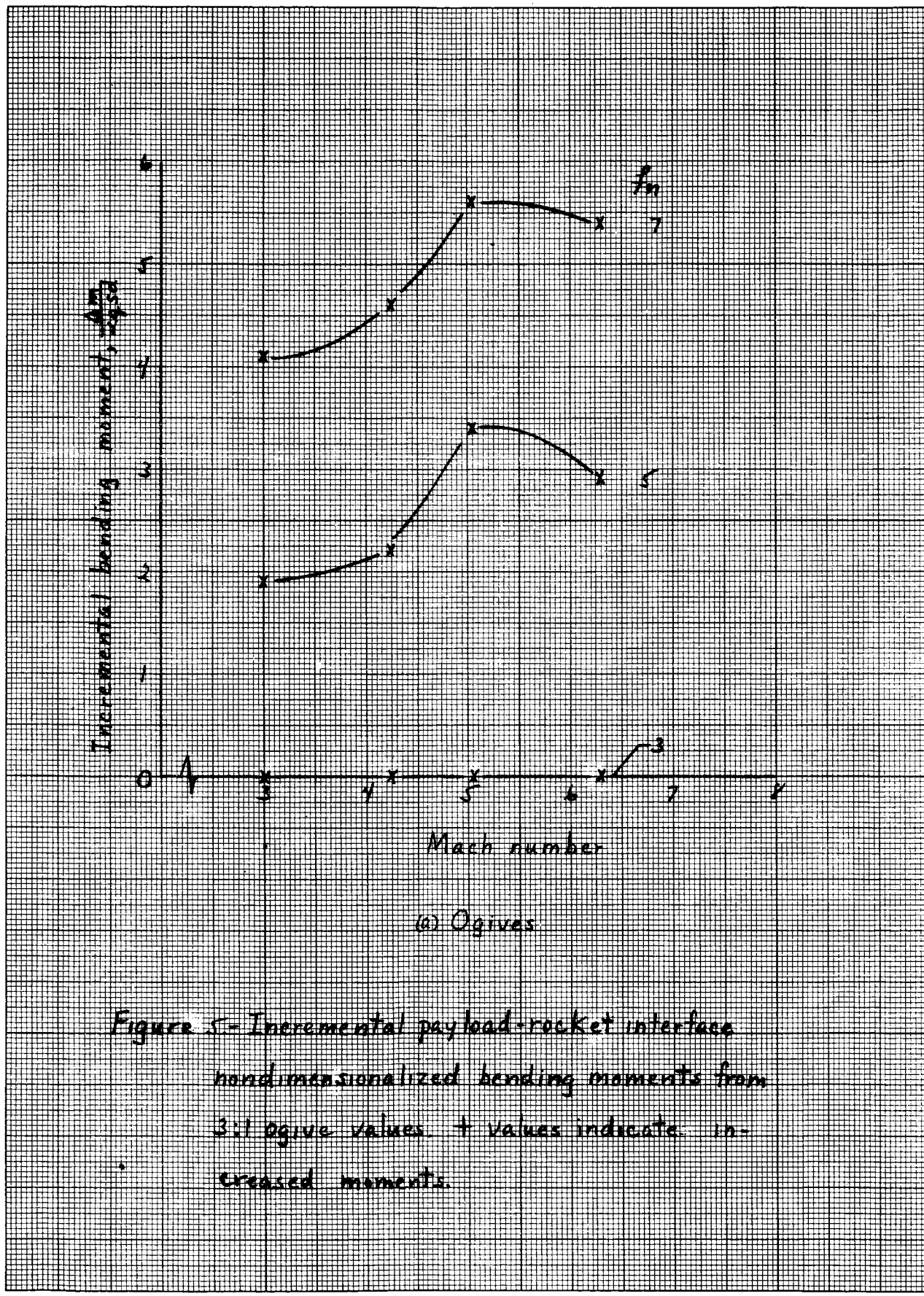

(a) Ogives

Figure 5- Incremental payload-rocket interface nondimensionalized bending moments from 3:1 ogive values. + values indicate increased moments.

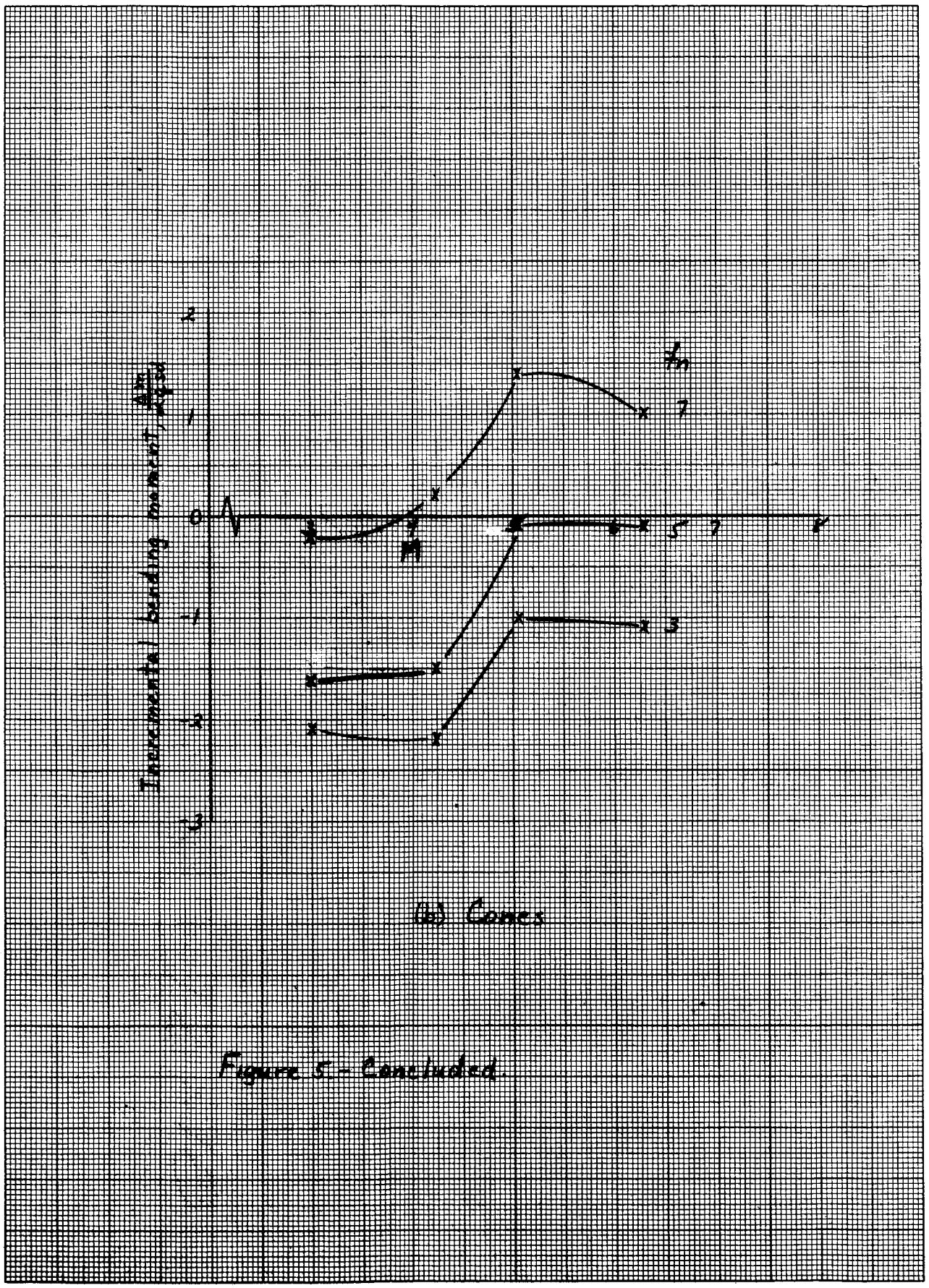

(b) Cones

Figure 5 - Concluded.

OPTIONAL FORM NO. 10
MAY 1962 EDITION
GSA GEN. REG. NO. 27
5010-107

UNITED STATES GOVERNMENT

Memorandum

TO : Flight Performance Section Files DATE: 4 November 1965

FROM : Mr. Edward E. Mayo
Flight Performance Section

SUBJECT: NOSE OPTIMIZATION STUDY, PART II - STABILITY AND PAYLOAD-ROCKET INTERFACE BENDING MOMENTS, CASE II

REFERENCE:
(a) Memo of 27 August 1965, Mr. George A. Weisskopf to Flight Performance Section Files, Subject: Nose Optimization Study, Part I - Comparative Performance of Tangent Ogive and Conical Noses
(b) Memo of 11 October 1965, Mr. Edward E. Mayo to Flight Performance Section Files, Subject: Nose Optimization Study, Part II - Stability and Payload-Rocket Interface Bending Moments, Case I
(c) Memo of 29 June 1965, Mr. Edward E. Mayo to Flight Performance Section Files, Subject: Effect of Payload Weight on the Tomahawk Mass, Static Margin, Static Stability, and Natural Frequency Characteristics
(d) Memo of 7 July 1965, Mr. Edward E. Mayo to Flight Performance Section Files, Subject: Cone-Cylinder and Ogive-Cylinder Geometric and Mass Characteristics
(e) Syverston, Clarence A. and Dennis, David H.: A Second-Order Shock-Expansion Method Applicable to Bodies of Revolution Near Zero Lift. NACA Report 1328, 1957

INTRODUCTION

This memorandum is a continuation of the nose optimization studies presented in references (a) and (b). Reference (a) is a delineation of the effects of nose shape on apogee altitude. Reference (b) investigates the vehicle stability and payload-rocket interface bending moments for payload weight distribution Case I (constant density payload contained within the payload cylindrical section). The study presented herein examines the vehicle stability and payload-rocket interface bending moments for payload weight distribution Case II (constant volume, constant density payload; see figure 1). It is believed that these two cases should bracket actual weight distributions; and, hence, if the same conclusions can be drawn from these cases, they should also apply for the actual distribution.

ANALYSIS

Trajectory and mass characteristics. - The pertinent trajectory characteristics, Mach number and dynamic pressure, are given in figure 2 for the extreme nose shapes (f_n = 3 ogive and f_n = 7 cone) as obtained from reference (b). The invariancy of these characteristics with nose shape allows, as shown in reference (b), direct comparison of changes in stability and payload-rocket interface bending moments as a function of only Mach number. The vehicle weight, center-of-gravity location and pitch moment of inertia are presented in figure 3. The vehicle without payload mass characteristics of reference (c) were combined with the payload mass characteristics of reference (d) to obtain the values in figure 3.

Stability. - The stability characteristics for the vaious nose configurations were determined by modifying the Tomahawk configuration (figure 1, reference (b), f_n = 3 ogive) aerodynamics which are given in table I. The fin + interference characteristics were obtained by utilizing the f_n = 3 ogive, f_a = 10 body characteristics of table II(a). The fin + interference values are given by

$$C_{N_{\alpha(f+i)}} = C_{N_{\alpha}} - C_{N_{\alpha(n+a)}} \Big|_{\substack{f_n = 3 \text{ ogive} \\ f_a = 10}} \tag{1}$$

$$(x_{cp}/d)_{(f+i)} = \frac{C_{N_\alpha}(x_{cp}/d) - \left[C_{N_{\alpha(n+a)}} (x_{cp}/d)_{(n+a)}\right]_{\substack{f_n=3 \text{ ogive} \\ f_a=10}}}{C_{N_{\alpha(f+i)}}} \tag{2}$$

The vehicle stability characteristics were then obtained by combining the fin + interference values with the various fineness ratio nose values of table II(a). The vehicle stability equations are

$$C_{N_\alpha} = C_{N_{\alpha(f+i)}} + C_{N_{\alpha(n+a)}} \Big|_{f_a = 10} \tag{3}$$

$$x_{cp}/d = \frac{C_{N_{\alpha(f+i)}} (x_{cp}/d)_{(f+i)} + \left[C_{N_{\alpha(n+a)}} (x_{cp}/d)_{(n+a)}\right]_{f_a=10}}{C_{N_\alpha}} \tag{4}$$

The resulting stability characteristics are given in table III and incremental static margins from the $f_n = 3$ ogive values are presented in figure 4. For ogives (figure 4a), the $f_n = 3$ yields the greatest stability at the higher Mach numbers; whereas, at the lower Mach numbers, the higher fineness ratio ogives yield greater stability. For cones (figure 4b), the higher fineness ratio noses yield greater stability. For the Tomahawk, the Mach number for minimum stability is about 8; hence, figure 4 indicates that the $f_n = 3$ ogive yields the largest minimum static margin. The only competitive shape is the 7:1 cone-cylinder payload; however, since its probable density distribution is more accurately approximated by payload weight distribution Case I considered in reference (b), the 3:1 ogive-cylinder payload is considered the best shape at M = 8.

Payload-rocket interface bending moments. - The payload-rocket interface bending moments were assumed to be composed of aerodynamic, rotational inertia and translational components, i.e.,

$$\frac{m}{\alpha qsd} = \left|\frac{m}{\alpha qsd}\right|_{\substack{\text{Aerodynamic} \\ \text{Rotational} \\ \text{Inertia}}} + \left|\frac{m}{\alpha qsd}\right|_{\substack{\text{Translational} \\ \text{Inertia}}} \tag{5}$$

which may be expressed as

$$\frac{m}{\alpha qsd} = C_{N_{\alpha_{(n+a)}}}\Big|_{\text{table II(b)}}\left[f_n + f_a - \left(\frac{\bar{x}_{cp}}{d}\right)_{(n+a)}\right]_{\text{table II(b)}} - \frac{(I_p)_{p.i.}}{I} C_{m_\alpha}$$

$$- \frac{W_p}{W} C_{N_\alpha}\left[f_n + f_a - (\bar{x}_{cg}/d)_p\right]_{\text{table II(b)}} \tag{6}$$

The resulting nondimensionalized bending moments are summarized in table IV and the incremental nondimensionalized bending moments from the $f_n = 3$ ogive values are shown in figure 5. From figure 5, the higher fineness ratio noses tend to yield lower payload-rocket interface bending moments.

SUMMARY AND CONCLUSIONS

In summary, the results of this study indicate that for the Nike Tomahawk vehicle, the optimum nose shape from stability considerations is the 3:1 ogive; whereas, from bending moment considerations, the optimum nose is the 7:1 cone.

In conclusion, the results of the Nike Tomahawk vehicle nose optimization studies (references (a), (b) and the study presented herein) may be summarized as follows:

1. The differences in apogee altitude between the $f_n = 3$ ogive and $f_n = 7$ cone is only 12 miles in 200 (6%).

2. The optimum nose shape from stability considerations is the $f_n = 3$ ogive.

3. The optimum nose shape from payload-rocket interface bending moment considerations depends upon the mass distribution of the payload. For constant density payloads contained within the payload cylindrical section, the $f_n = 3$ cone yields the lowest payload-rocket interface bending moment; whereas, for constant volume - constant density payloads, the fineness ratio 7 cone yields the lowest payload-rocket interface bending moment.

Edward E. Mayo

Edward E. Mayo

Enclosures:
(1) Symbols
(2) Tables (4)
(3) Figures (5)

cc: Mr. K. R. Medrow
Mr. G. E. MacVeigh
Mr. E. E. Bissell
Miss E. C. Pressly
Mr. N. E. Peterson, Jr.

EEM:skd

SYMBOLS

$C_{N_{\alpha}}$	normal force coefficient curve slope at $\alpha = 0$, per radian
d	reference diameter, d = 0.75 ft.
f	fineness ratio
I	pitch inertia
M	free-stream Mach number
m	bending moment at payload-rocket interface
q	free-stream dynamic pressure
S	reference area, $S = \frac{\pi d^2}{4}$
S.M.	static margin, minus for positive stability
t	time, sec.
x	longitudinal distance measured forward of base
$\bar{x}$	longitudinal distance measured aft of nose apex
W	weight
α	angle of attack, radians

SUBSCRIPTS

a	cylindrical afterbody
cg	center-of-gravity location
cp	center-of-pressure location
n	nose
p	payload
p.i.	payload interface

Table I. - Aerodynamic Characteristics of Tomahawk Sounding Rocket.*
f_n = 3 ogive.

Mach	C_{N_α}	x_{cp}, feet
3.00	14.10	4.002
4.24	11.14	5.015
5.05	10.20	5.530
6.28	9.37	6.170

* Reference (c)

Table II. - Aerodynamic Characteristics of Tangent Ogive-Cylinder and Cone-Cylinder Configurations.*

(a) $f_a = 10$

$C_{N_{\alpha}}{}_{(n+a)}$

	Ogives			Cones		
M \ f_n	3	5	7	3	5	7
3.00	3.32	3.06	2.85	3.37	3.01	2.84
4.24	3.34	3.18	3.11	3.45	3.21	2.85
5.05	3.38	3.29	3.02	3.63	3.26	3.06
6.28	2.90	3.31	3.24	3.37	3.22	2.99

$(\bar{x}_{cp}/d)_{(n+a)}$

	Ogives			Cones		
M \ f_n	3	5	7	3	5	7
3.00	2.60	3.75	4.55	3.51	4.88	6.32
4.24	3.12	4.09	5.16	3.82	5.39	6.39
5.05	3.60	4.06	5.23	3.82	5.25	6.55
6.28	3.05	4.32	5.58	3.77	5.32	6.74

*Experimental data of reference (e).

Table II. - Concluded

(b) Equal Volume

	Ogives			Cones		
f_n	3	5	7	3	5	7
f_a	4.44	3.37	2.35	5.05	4.41	3.73
$(\bar{x}_{cg}/d)_p$	4.38	5.25	6.13	5.00	6.28	7.46
M	$(C_{N_\alpha})_{n+a}$					
3.00	3.29	2.90	2.75	3.19	2.91	2.70
4.24	3.20	2.90	2.70	3.20	2.90	2.67
5.05	3.09	2.90	2.79	3.27	2.90	2.68
6.28	2.67	2.75	2.69	3.10	2.80	2.54

	Ogives			Cones		
f_n	3	5	7	3	5	7
f_a	4.44	3.37	2.35	5.05	4.41	3.73
$(\bar{x}_{cg}/d)_p$	4.38	5.25	6.13	5.00	6.28	7.46
M	$(\bar{x}_{cp}/d)_{(n+a)}$					
3.00	2.45	3.25	4.14	3.10	4.45	5.69
4.24	2.55	3.45	4.20	3.30	4.70	5.95
5.05	2.90	3.60	4.35	3.30	4.65	5.85
6.28	2.50	3.50	4.28	3.40	4.65	5.75

Table III. - Aerodynamic Characteristics of Tomahawk Sounding Rocket with Various Fineness Ratio Noses

(a) Ogives

M	t_s, sec	C_{N_α}	S.M. Calibers	Δ S.M.* Calibers
$f_n = 3$				
3	2.2	14.10	-4.63	0
4.24	3.85	11.14	-3.46	0
5.05	4.83	10.20	-2.91	0
6.28	6.27	9.37	-2.28	0
$f_n = 5$				
3	2.2	13.84	-4.98	-.35
4.24	3.85	10.98	-3.68	-.22
5.05	4.83	10.11	-2.87	+.04
6.28	6.27	9.78	-1.92	+.36
$f_n = 7$				
3	2.2	13.63	-5.20	-.57
4.24	3.85	10.91	-3.81	-.35
5.05	4.83	9.84	-3.30	-.39
6.28	6.27	9.71	-2.14	+.14

*Δ S.M. = S.M.$\Big|_{f_n}$ - S.M.$\Big|_{f_n = 3 \text{ ogive}}$. + indicates decreased stability

Table III. - Concluded

(b) Cones

M	t, sec	C_{N_α}	S.M. Calibers	Δ S.M.* Calibers
$f_n = 3$				
3	2.2	14.15	-4.66	-.03
4.24	3.85	11.25	-3.36	+.10
5.05	4.83	10.45	-2.47	+.44
6.28	6.27	9.84	-1.75	+.53
$f_n = 5$				
3	2.2	13.79	-5.07	-.44
4.24	3.85	11.01	-3.73	-.27
5.05	4.83	10.08	-2.96	-.05
6.28	6.27	9.69	-2.01	+.27
$f_n = 7$				
3	2.2	13.62	-5.30	-.67
4.24	3.85	10.65	-4.11	-.65
5.05	4.83	9.88	-3.24	-.33
6.28	6.27	9.46	-2.37	-.09

*Δ S.M. = S.M.$|_{f_n}$ - S.M.$|_{f_n = 3 \text{ ogive}}$ + indicates decreased stability

Table IV. - Payload-Rocket Interface Non-Dimensionalized Bending Moment, $\frac{m}{\alpha qsd}$

(a) Ogives

Mach	t, sec (m/αqsd)	Aero.	Rotational Inertia	Translational Inertia	Total	Δm*/αqsd
$f_n = 3$						
3	2.2	16.42	4.68	9.58	11.52	0
4.24	3.85	15.65	2.94	8.89	9.70	0
5.05	4.83	14.03	2.35	9.08	7.30	0
6.28	6.27	13.19	1.79	9.75	5.23	0
$f_n = 5$						
3	2.2	14.85	5.13	9.59	10.39	-1.13
4.24	3.85	14.27	3.21	8.94	8.54	-1.16
5.05	4.83	13.83	2.39	9.18	7.04	- .26
6.28	6.27	13.39	1.62	10.37	4.64	- .59
$f_n = 7$						
3	2.2	14.33	5.74	9.74	10.33	-1.19
4.24	3.85	13.90	3.51	9.17	8.24	-1.46
5.05	4.83	13.95	2.90	9.22	7.63	+ .33
6.28	6.27	13.64	1.95	10.63	4.96	- .27

* $\frac{\Delta m}{\alpha qsd} = \frac{m}{\alpha qsd}\Big|_{f_n} - \frac{m}{\alpha qsd}\Big|_{f_n = 3 \text{ ogive}}$

Table IV. - Concluded

(b) Cones

Mach	m/α qsd / t, sec	Aero.	Rotational Inertia	Translational Inertia	Total	$\frac{\Delta m^*}{\alpha}$ qsd
			$f_n = 3$			
3	2.2	15.79	4.70	-9.58	10.91	- .61
4.24	3.85	15.20	2.87	-8.96	9.17	- .59
5.05	4.83	15.53	2.03	-9.28	8.28	+ .98
6.28	6.27	14.41	1.43	-10.20	5.64	+ .41
			$f_n = 5$			
3	2.2	14.43	5.59	-9.58	10.44	-1.08
4.24	3.85	13.66	3.31	-8.99	7.98	-1.72
5.05	4.83	13.80	2.50	-9.18	7.12	- .18
6.28	6.27	13.33	1.72	-10.30	4.75	- .48
			$f_n = 7$			
3	2.2	13.61	6.02	-9.89	9.74	-1.78
4.24	3.85	12.76	3.88	-9.09	7.55	-2.15
5.05	4.83	13.08	2.94	-9.40	6.62	- .68
6.28	6.27	12.65	2.17	-10.52	4.30	- .93

* $\frac{\Delta m}{\alpha\ qsd} = \left.\frac{m}{\alpha qsd}\right|_{f_n} - \left.\frac{m}{\alpha qsd}\right|_{f_n = 3\ ogive}$

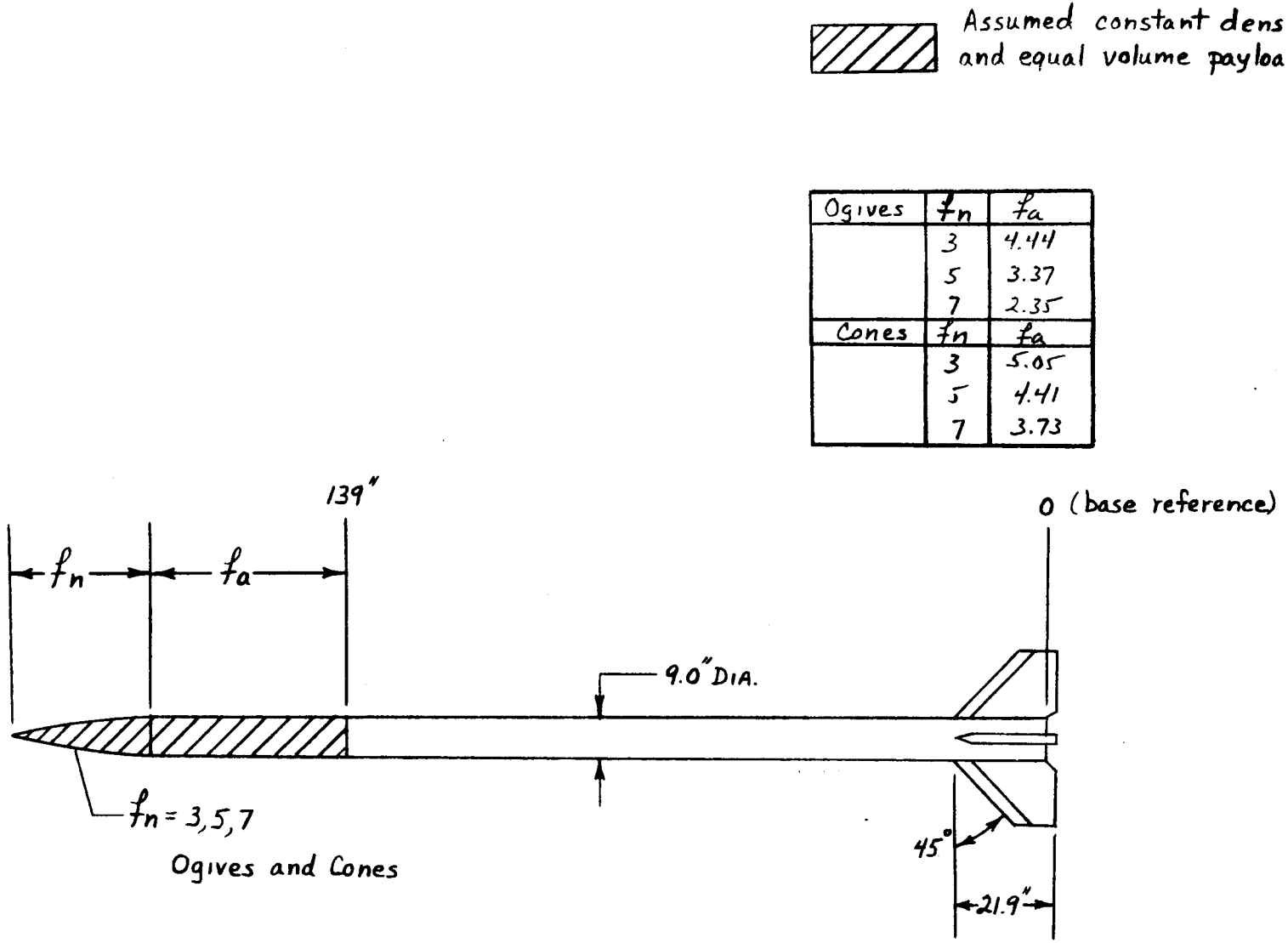

Payload weight distribution. Case II

Figure 1 - Tomahawk TE-416 sounding rocket. Gross payload weight = 123 lbs.

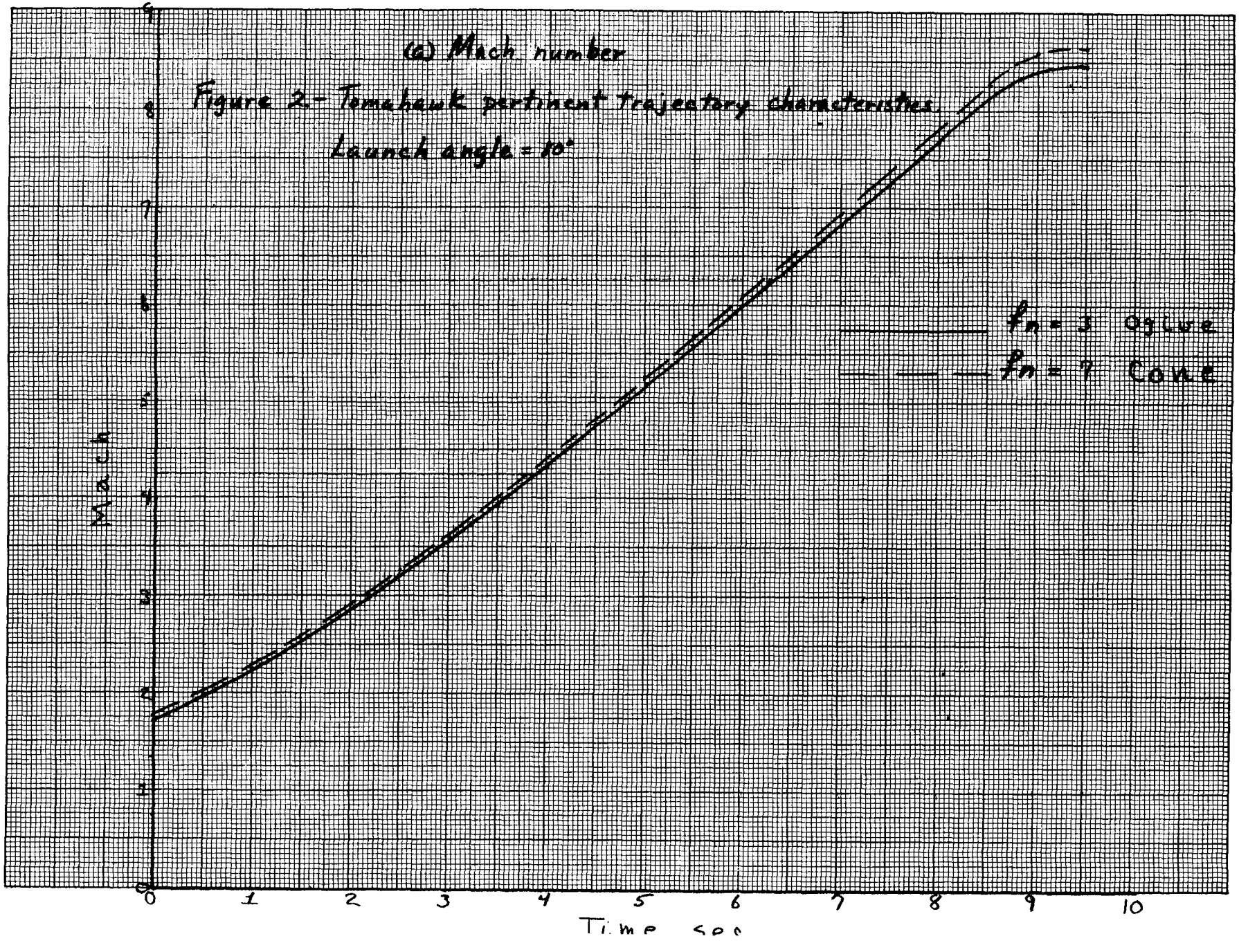
(a) Mach number
Figure 2.- Tomahawk pertinent trajectory characteristics.
Launch angle = 10°
f_n = 3 Ogive
f_n = 7 Cone
Mach No.
Time sec
0
1
2
3
4
5
6
7
8
9
10

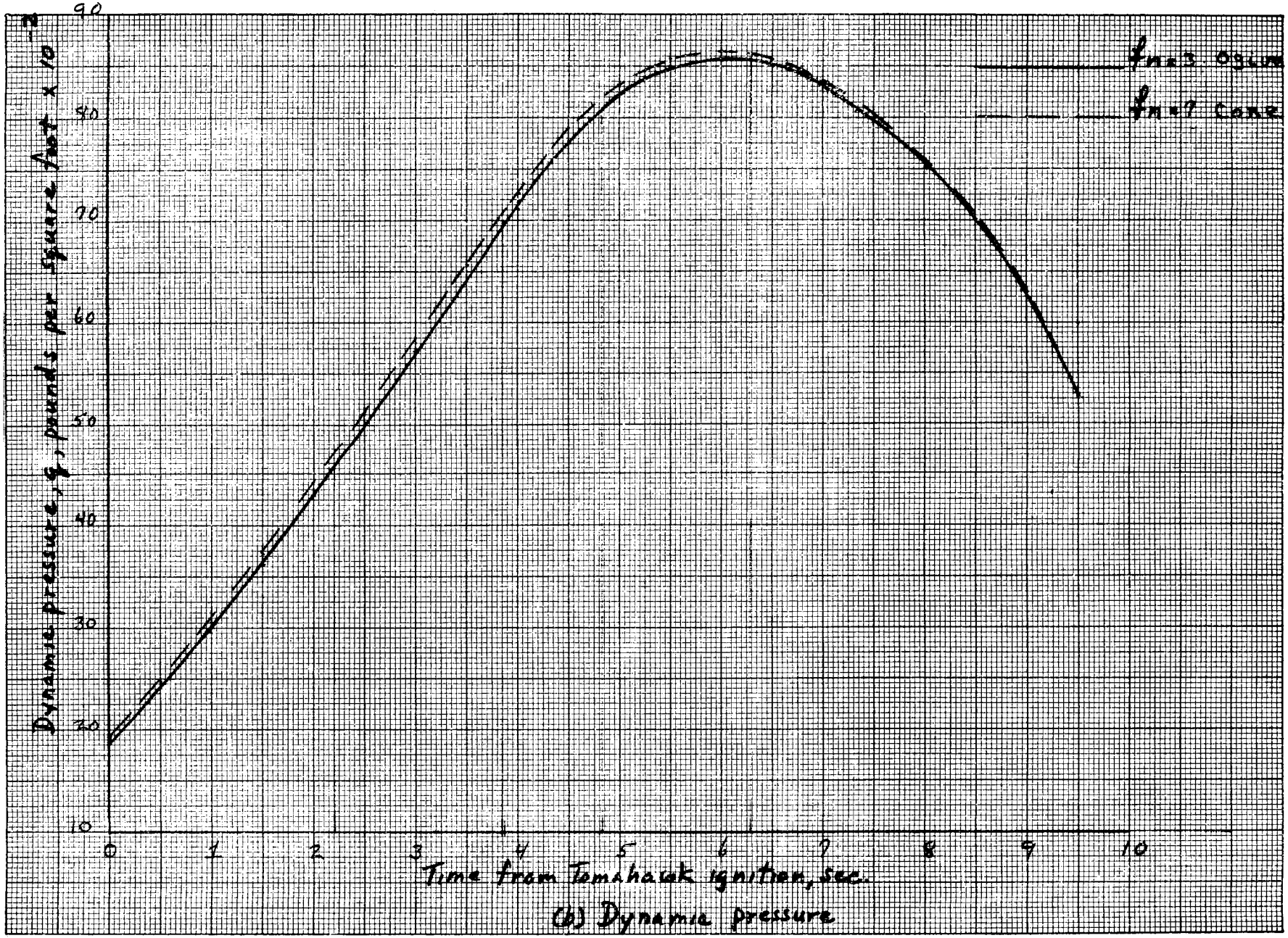

(b) Dynamic pressure.

Figure 2.- Concluded.

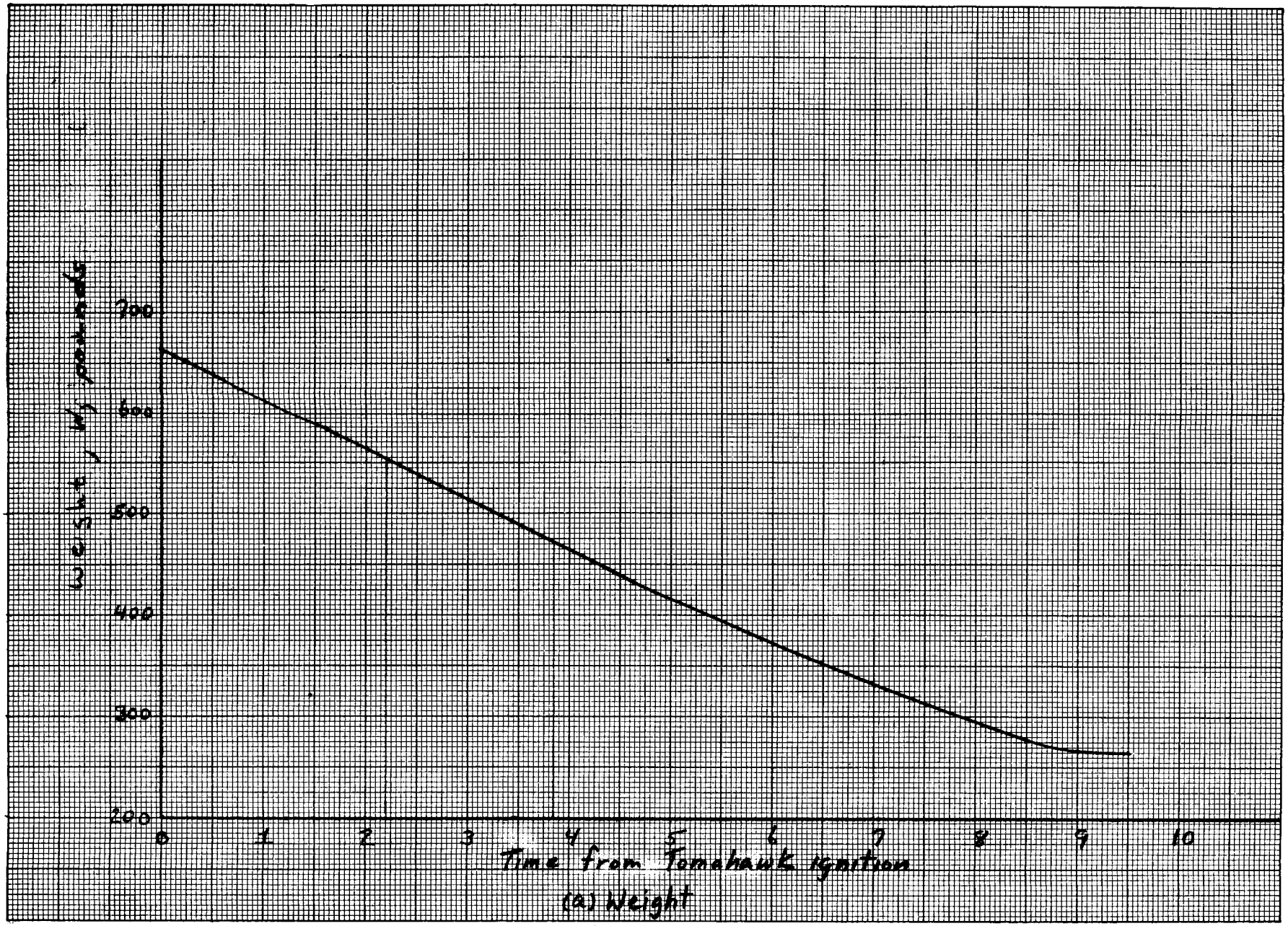

(a) Weight

Figure 3.- Tomahawk pertinent mass characteristics.

Figure 1.- Continued.

Figure 3.- Continued.

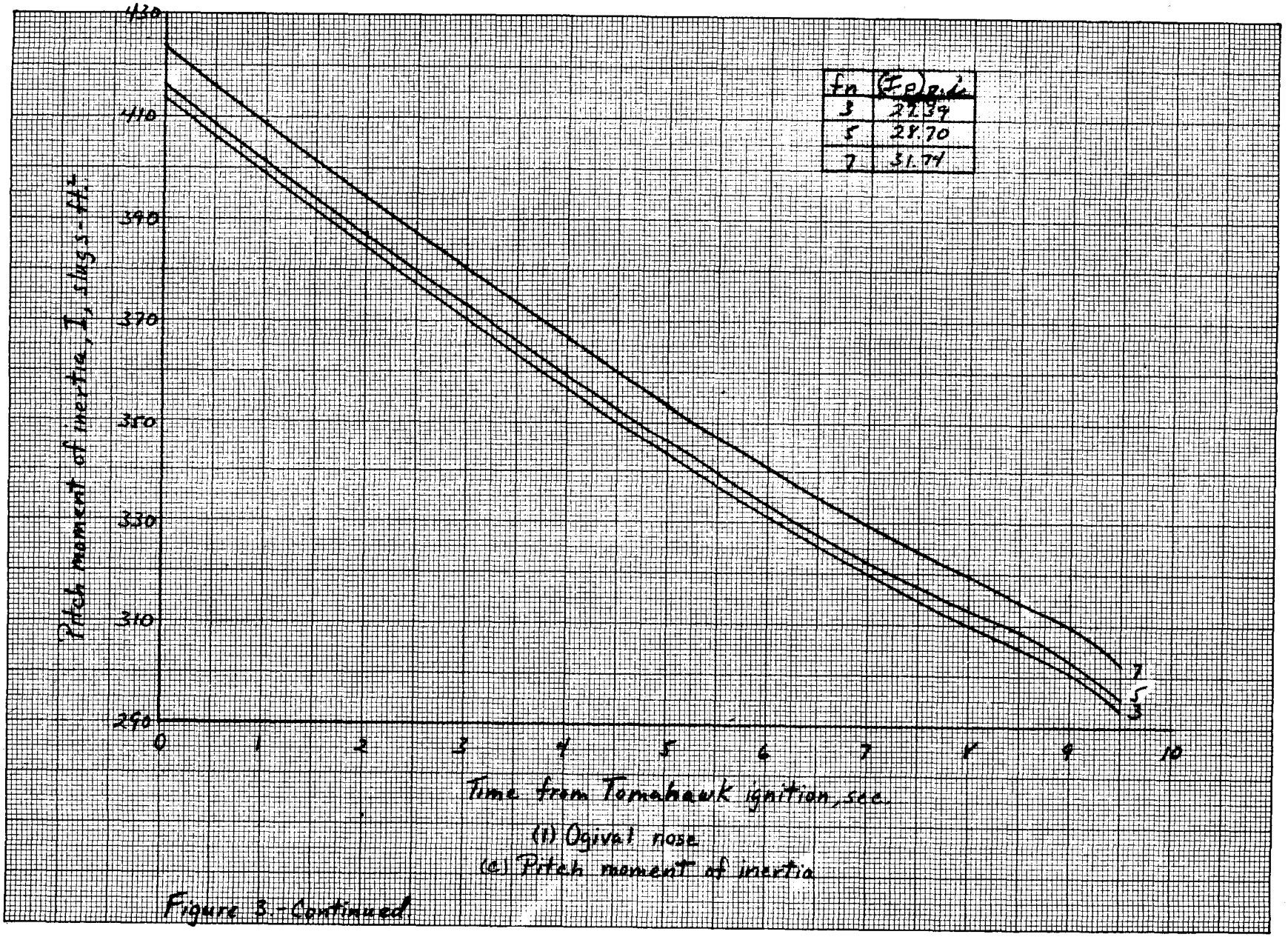

Figure 3.- Continued.

Time from Tomahawk ignition, sec
Pitch moment of inertia, I_y, slug-ft²
(a) Conical nose
(b) Concluded.
Figure 3.- Concluded.

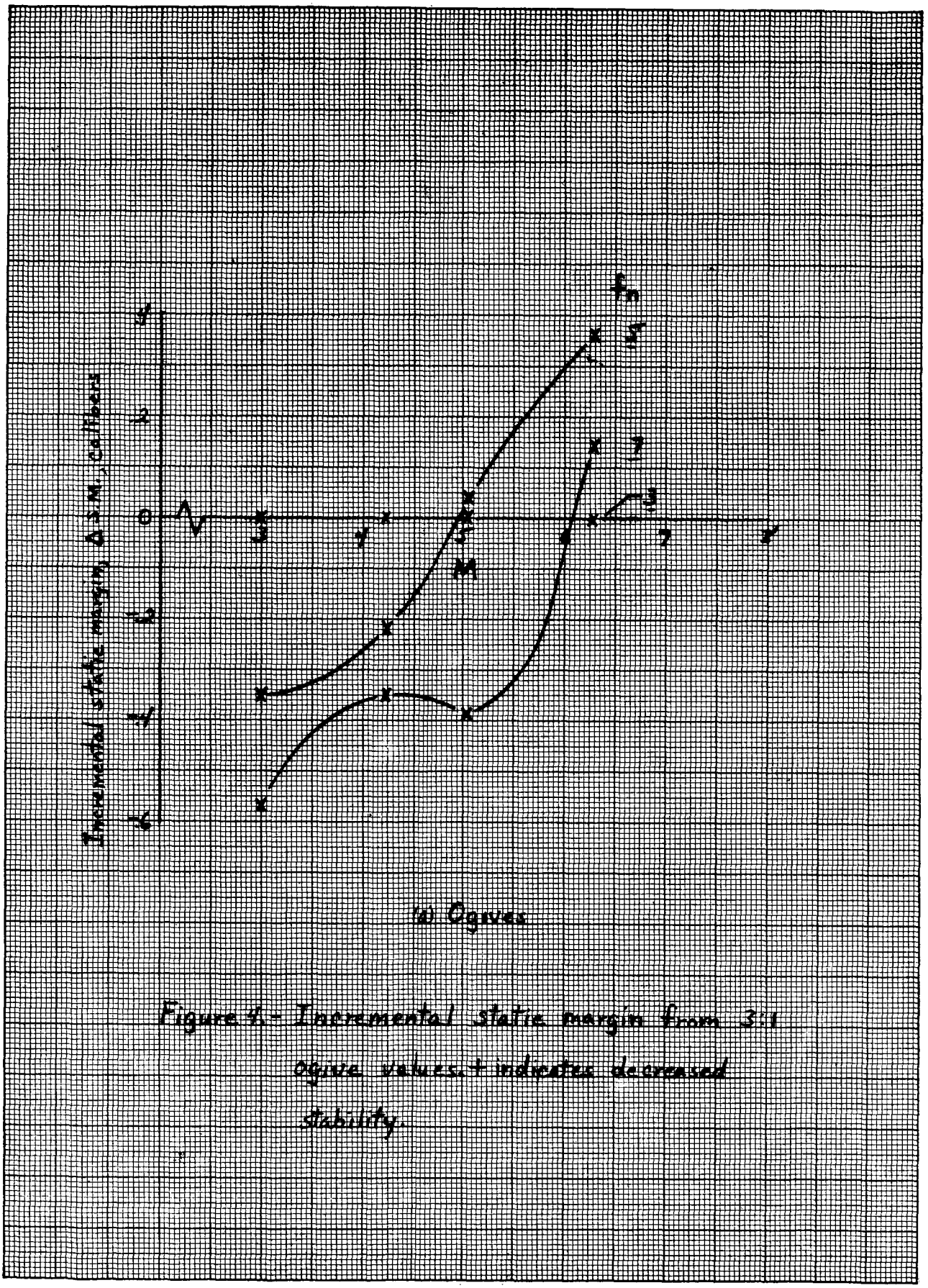

(a) Ogives

Figure 4.- Incremental static margin from 3:1 ogive values. + indicates decreased stability.

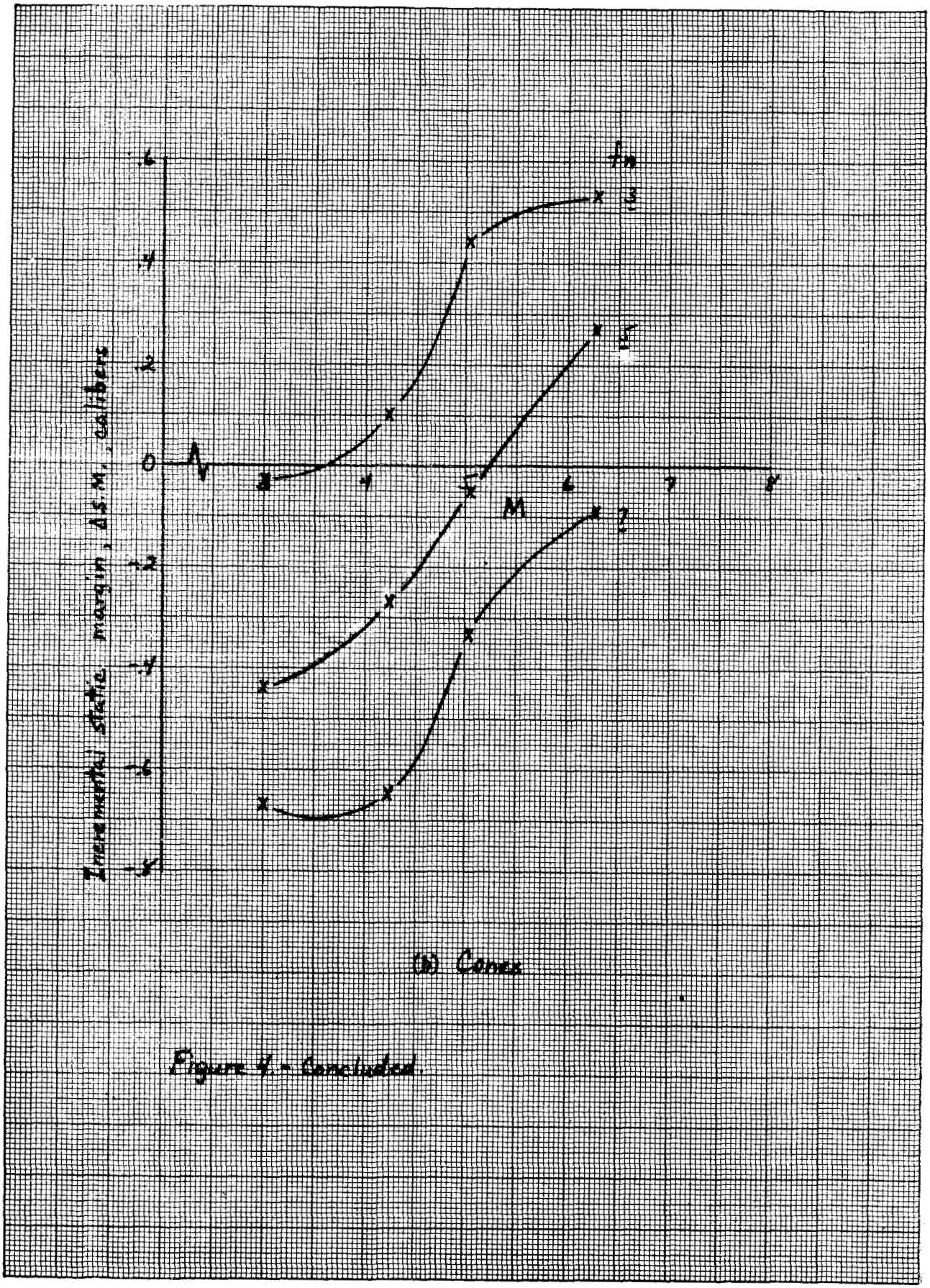

(b) Cones

Figure 4.- Concluded.

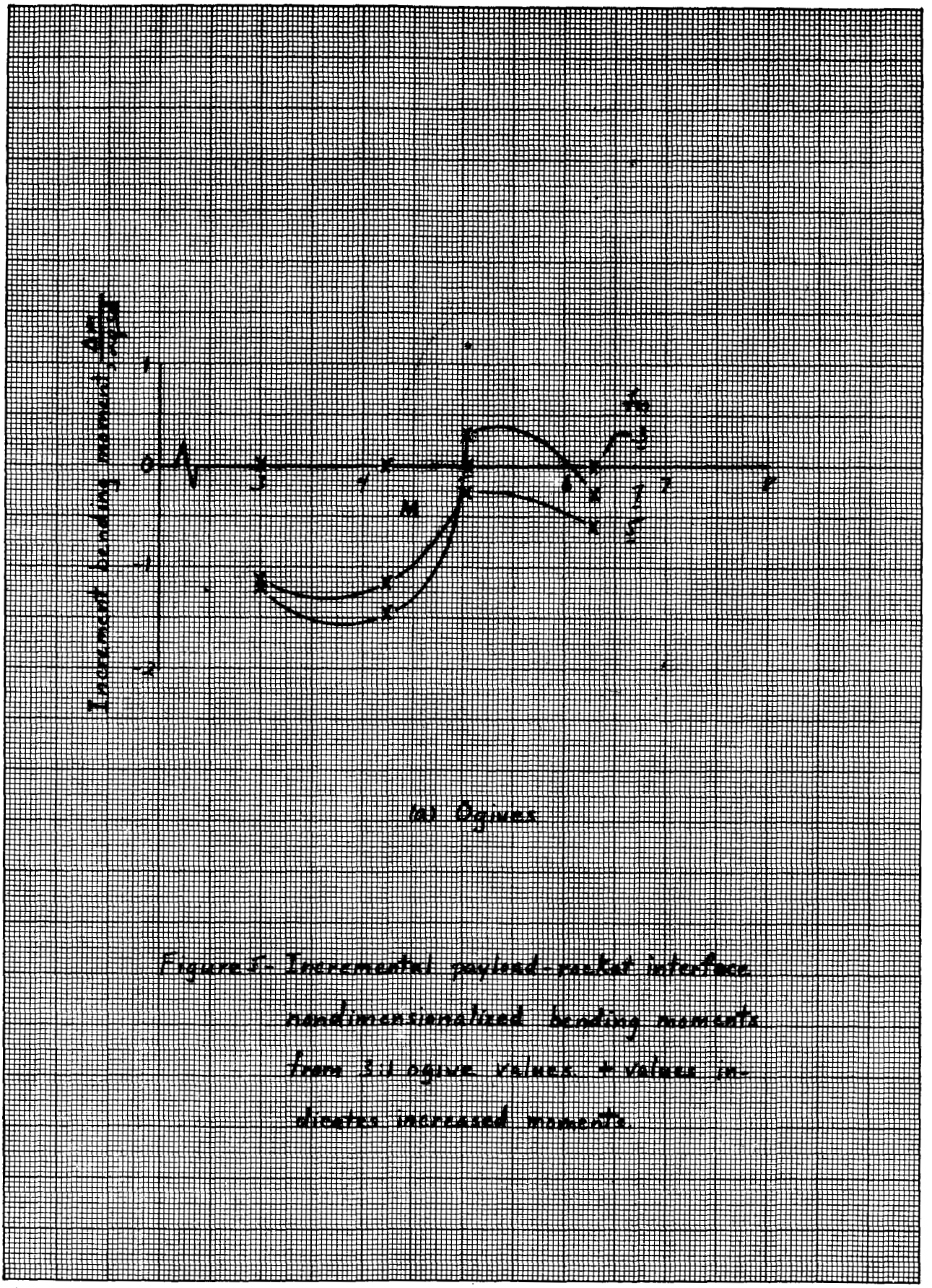

(a) Ogives

Figure 5.- Incremental payload-rocket interface nondimensionalized bending moments from 3 ogive values. + values indicates increased moments.

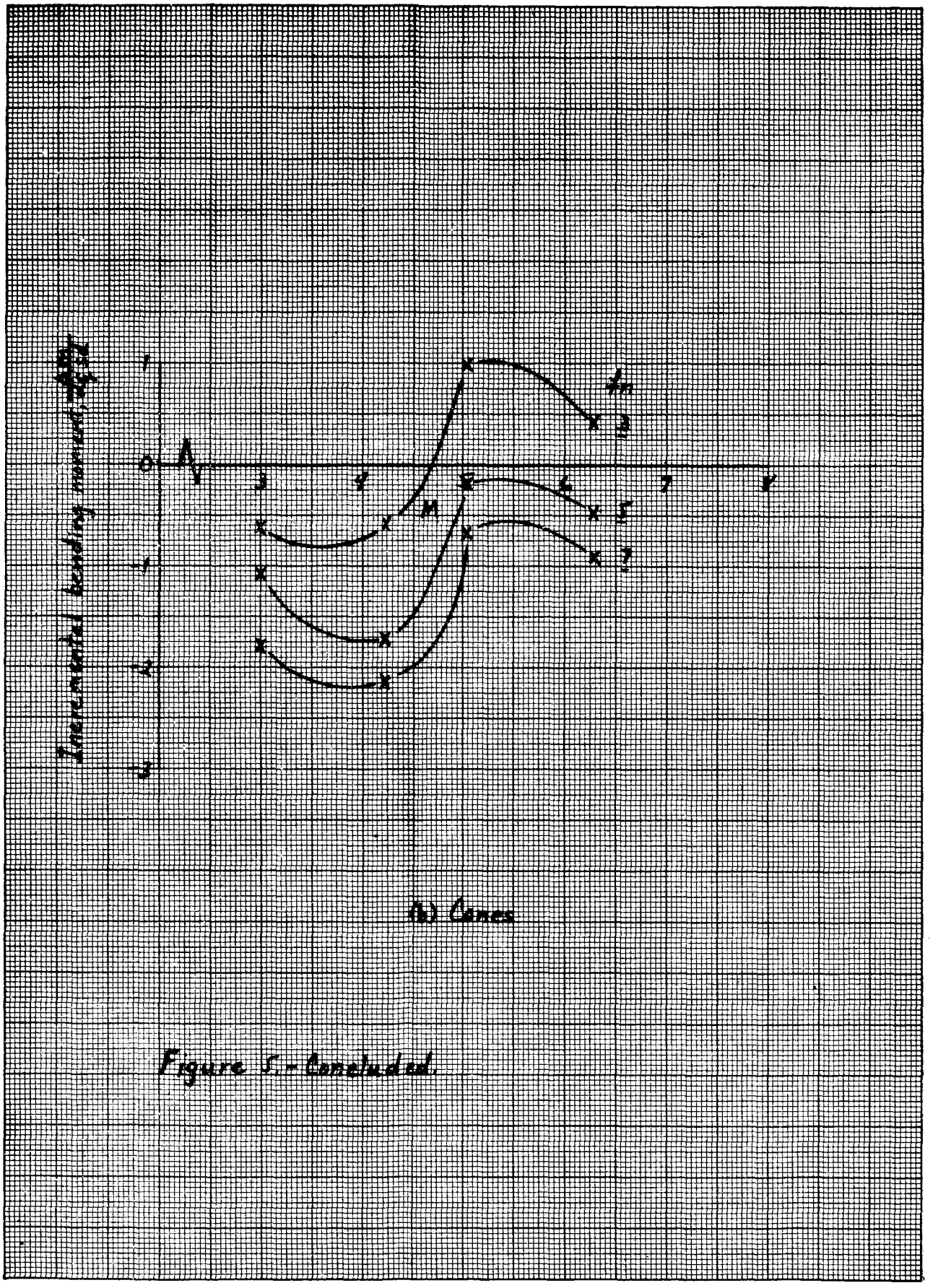

(b) Cones

Figure 5.- Concluded.

OPTIONAL FORM NO. 10
MAY 1962 EDITION
GSA GEN. REG. NO. 27
5010-107

UNITED STATES GOVERNMENT

Memorandum

TO : Flight Performance Section Files DATE: 7 July 1965

FROM : Mr. Edward E. Mayo and Mr. Carl I. Hutton, Jr.
Flight Performance Section

SUBJECT: TANGENT OGIVE GEOMETRIC AND MASS CHARACTERISTIC EQUATIONS

REFERENCE: (a) Pierce, B. O., and Foster, Ronald M.: A Short Table of Integrals. Fourth Edition.

INTRODUCTION

In a study currently underway to optimize the nose shape of sounding rockets, the nondimensionalized expressions for the geometric and mass characteristics of tangent ogives have been derived in terms of the ogive fineness ratio, f. The purpose of this memorandum is to document the expressions and an outline of their derivations. The expressions are being programmed by R. Lahn for evaluation.

EQUATIONS

Body Equations. - The surface ordinate and surface slope expressions are derived in Appendix A and summarized below.

$$\frac{\rho}{d} = \sqrt{(f^2 + \tfrac{1}{4})^2 - (x/d - f)^2} - (f^2 - \tfrac{1}{4})$$

$$\delta = \tan^{-1}\left[\frac{f - x/d}{\rho/d + f^2 - \tfrac{1}{4}}\right]$$

Volume. - The volume expression is derived in Appendix B and summarized below.

$$\frac{V}{\pi d^3} = f(f^2 + \tfrac{1}{4})^2 - 1/3f^3 - (f^2 - \tfrac{1}{4})(f^2 + \tfrac{1}{4})^2 \sin^{-1}\left(\frac{f}{f^2 + \tfrac{1}{4}}\right)$$

Center-of-Volume. - The center-of-volume expression is derived in Appendix C and summarized below.

$$(c.v./d)\ \frac{V}{\pi d^3} = \tfrac{1}{2}f^2(f^2 + \tfrac{1}{4})^2 - 1/12\ f^4$$

$$- 2(f^2 - \tfrac{1}{4})(f^2 + \tfrac{1}{4})^2\left[\tfrac{1}{2}f\sin^{-1}\left(\frac{f}{f^2 + \frac{1}{4}}\right) - 1/3\ (f^2 + \tfrac{1}{4})\right]$$

$$+ 2(f^2 - \tfrac{1}{4})^2\left[-\frac{(f^2 - \frac{1}{4})^2}{3} - \frac{f^2}{2}\right] + \tfrac{1}{2}f^2(f^2 - \tfrac{1}{4})^2$$

Mass Moment of Inertia. - The mass moment of inertia is derived in Appendix D and summarized below.

$$\frac{I}{\rho \pi d^5} = 1/3\ f^3(f^2 + \tfrac{1}{4})^2 - 1/30\ f^5 + 4/3\ f(f^2 + \tfrac{1}{4})^3(f^2 - \tfrac{1}{4})$$

$$- 5/6\ f(f^2 - \tfrac{1}{4})^4 - \left[5/4\ f^2(f^2 - \tfrac{1}{4}) + \tfrac{1}{4}(f^2 - \tfrac{1}{4})^3\right]$$

$$\left[f(f^2 - \tfrac{1}{4}) + (f^2 + \tfrac{1}{4})^2\ \sin^{-1}\left(\frac{f}{f^2 + \frac{1}{4}}\right)\right] + 1/3\ f^3(f^2 - \tfrac{1}{4})^2$$

Wetted Surface Area. - The wetted surface area is derived in Appendix E and summarized below.

$$\frac{S}{S_B} = 8(f^2 + \tfrac{1}{4})^2\left\{\sin\left[\tan^{-1}\left(\frac{f}{f^2 - \frac{1}{4}}\right)\right] - \left(1 - \frac{1}{2f^2 + 0.5}\right)\tan^{-1}\left(\frac{f}{f^2 - \frac{1}{4}}\right)\right\}$$

Edward E. Mayo

Carl I. Hutton, Jr.

Enclosures:
Appendixes A, B, C, D and E

cc: Mr. K. R. Medrow

EEM:skd

APPENDIX A

TANGENT OGIVE BODY EQUATIONS

The tangent ogive semi-cross section is shown encompassed by its arc circle (primed coordinates), as the cross hatched area in sketch (a).

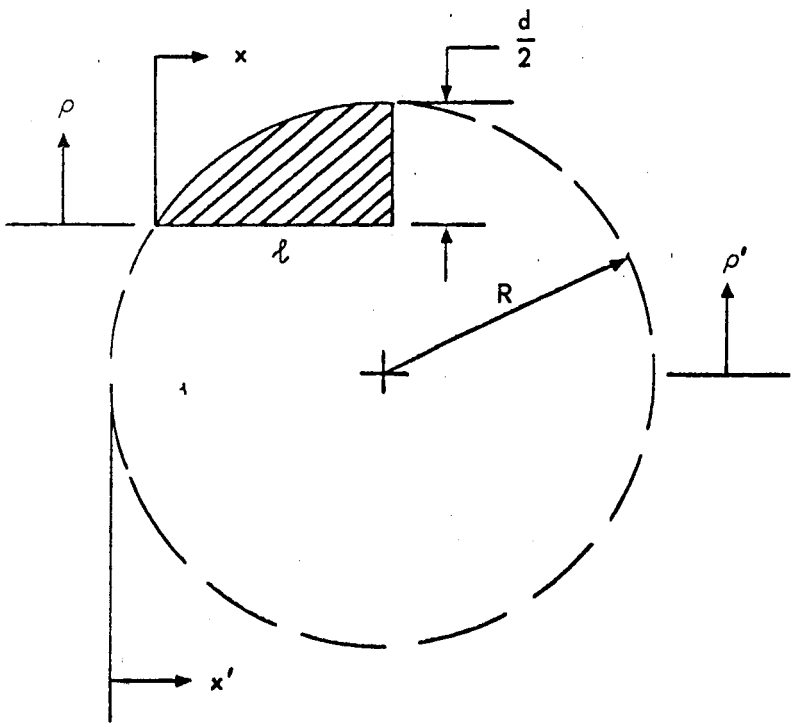

Sketch (a)

The equation of the arc circle in the primed coordinate system is given by

$$(x' - R)^2 + \rho'^2 = R^2 \qquad \text{(A1)}$$

The following relationships exist between the arc circle and the ogive coordinate systems:

$$x' = x + (R - \ell) \tag{A2}$$

$$\rho' = \rho + (R - d/2) \tag{A2}$$

Substitution of equations (A2 into equation (A1) and nondimentionalizing, yields

$$\left[x/d - f\right]^2 + \left[\rho/d + (R/d - 1/2)\right]^2 = (R/d)^2 \tag{A3}$$

which, upon solving for ρ/d, gives

$$\rho/d = \sqrt{(R/d)^2 - (x/d - f)^2} - (R/d - 1/2)$$

Making use of the relation

$$(R/d)^2 = f^2 + (R/d - 1/2)^2 \tag{A4}$$

leads to the following expression for ρ/d:

$$\rho/d = \sqrt{(f^2 + 1/4)^2 - (x/d - f)^2} - (f^2 - 1/4) \tag{A5}$$

The surface slope, δ, is given by

$$\delta = \tan^{-1} \frac{d(\rho/d)}{d(x/d)} \tag{A6}$$

Differentiation of equation (A3) according to equation (A6), and making use of equation (A4), yields the following relation for

$$\delta = \tan^{-1} \left[\frac{f - (x/d)}{\rho/d + f^2 - 1/4}\right] \tag{A7}$$

APPENDIX B

TANGENT OGIVE VOLUME

The nondimensionalized volume integral for the tangent ogive may be expressed as

$$\frac{V}{\pi d^3} = \int_o^f (\rho/d)^2 \, d(x/d) \tag{B1}$$

where ρ/d was derived in appendix A and is given by equation (A5) as

$$\rho/d = \sqrt{(f^2 + 1/4)^2 - (x/d - f)^2} \quad - (f^2 - 1/4)$$

Hence, $(\rho/d)^2$ may be expressed in the following form

$$(\rho/d)^2 = (f^2 + 1/4)^2 - (x/d - f)^2 - 2(f^2 - 1/4)$$
$$\sqrt{- (x/d)^2 + 2f(x/d) + (f^2 - 1/4)^2} + (f^2 - 1/4)^2 \tag{B2}$$

Letting

$$A = \int_o^f (f^2 + 1/4)^2 \, d(x/d)$$

$$B = \int_o^f (x/d - f)^2 \, d(x/d)$$

$$C = 2(f^2 - 1/4) \int_o^f \sqrt{- (x/d)^2 + 2f(x/d) + (f^2 - 1/4)^2} \, d(x/d)$$

$$D = \int_o^f (f^2 - 1/4)^2 \, d(x/d)$$

Then

$$\frac{V}{\pi d^3} = A - B - C + D \tag{B3}$$

Where

$$A = \int_o^f (f^2 + 1/4)^2 \, d(x/d) = (f^2 + 1/4)^2 \, f \tag{B4}$$

$$B = \int_o^f (x/d - f)^2 \, d(x/d) = 1/3 \, f^3 \tag{B5}$$

$$C = 2(f^2 - 1/4) \int_o^f \sqrt{-(x/d)^2 + 2f(x/d) + (f^2 - 1/4)^2}\, d(x/d)$$

which, via formulas 170 and 166, p. 26, Pierce integral tables, may be expressed as follows

$$C = (f^2 - 1/4) \left\{ f(f^2 - 1/4) + (f^2 + 1/4)^2 \sin^{-1} \left[\frac{f}{(f^2 + 1/4)} \right] \right\} \quad \text{(B6)}$$

$$D = \int_o^f (f^2 - 1/4)^2\, d(x/d) = f(f^2 - 1/4)^2 \quad \text{(B7)}$$

Substitution of equations B4, B5, B6 and B7 into B3 yields

$$\frac{V}{\pi d^3} = f(f^2 + 1/4)^2 - 1/3\, f^3 - (f^2 - 1/4)(f^2 + 1/4)^2 \sin^{-1} \left(\frac{f}{f^2 + 1/4} \right) \quad \text{(B8)}$$

APPENDIX C

TANGENT OGIVE CENTER-OF-VOLUME

The nondimensionalized center-of-volume, (c.v./d), measured from the nose, is given by

$$c.v./d = \frac{\int_o^f (x/d)(\rho/d)^2 \, d(x/d)}{\int_o^f (\rho/d)^2 \, d(x/d)} \tag{C1}$$

where the numerator in the nondimensionalized volume moment integral, $M/\pi d^4$, and the denominator is the nondimensionalized volume integral, $V/\pi d^3$, evaluated in appendix B.

The volume moment integral, $M/\pi d^4$, from above, is given by

$$M/\pi d^4 = \int_o^f (x/d)(\rho/d)^2 \, d(x/d) \tag{C2}$$

where $(x/d)(\rho/d)^2$ may be expressed via equation B2 as

$$(x/d)(\rho/d)^2 = (f^2 + 1/4)^2(x/d) - (x/d - f)^2(x/d) - 2(f^2 - 1/4)(x/d)\sqrt{-(x/d)^2 + 2f(x/d) + (f^2 - 1/4)^2} + (f^2 - 1/4)^2(x/d) \tag{C3}$$

Letting

$$A = \int_o^f (f^2 + 1/4)^2 \, (x/d) \, d(x/d)$$

$$B = \int_o^f (x/d - f)^2 \, (x/d) \, d(x/d)$$

$$C = \int_o^f 2(f^2 - 1/4)(x/d)\sqrt{-(x/d)^2 + 2f(x/d) + (f^2 - 1/4)^2} \, d(x/d)$$

$$D = \int_o^f (f^2 - 1/4)^2 \, (x/d) \, d(x/d)$$

Then,

$$\frac{M}{\pi d^4} = A - B - C + D \tag{C4}$$

Where

$$A = \int_o^f (f^2 + 1/4)^2 \, (x/d) \, d(x/d) = 1/2 \, f^2(f^2 + 1/4)^2 \qquad (C5)$$

$$B = \int_o^f (x/d - f)^2 \, (x/d) \, d(x/d) = 1/12 \, f^4 \qquad (C6)$$

$$C = \int_o^f 2(f^2 - 1/4)(x/d) \sqrt{- (x/d)^2 + 2f(x/d) + (f^2 - 1/4)^2} \; d(x/d)$$

which, via formulas 181, 170 and 165, Pierce integral tables, may be expressed as follows

$$C = 2(f^2 - 1/4)(f^2 + 1/4)^2 \left[(1/2)f \sin^{-1} \left(\frac{f}{f^2 + 1/4}\right) - 1/3 \, (f^2 + 1/4)\right]$$

$$- 2(f^2 - 1/4)^2 \left[-\frac{(f^2 - 1/4)^2}{3} - \frac{f^2}{2}\right] \qquad (C7)$$

$$D = \int_o^f (f^2 - 1/4)^2 \, (x/d) \, d(x/d) = 1/2 \, f^2(f^2 - 1/4)^2 \qquad (C8)$$

Substitution of equations C5, C6, C7 and C8 into C4 yields

$$\frac{M}{\pi d^4} = 1/2 \, f^2(f^2 + 1/4)^2 - 1/12 \, f^4$$

$$- 2(f^2 - 1/4)(f^2 + 1/4)^2 \left[(1/2)f \sin^{-1} \left(\frac{f}{f^2 + 1/4}\right) - 1/3 \, (f^2 + 1/4)\right]$$

$$+ 2(f^2 - 1/4)^2 \left[-\frac{(f^2 - 1/4)^2}{3} - \frac{f^2}{2}\right] + 1/2 \, f^2(f^2 - 1/4)^2 \qquad (C9)$$

Hence, the nondimensionalized center-of-volume is given by

$$c.v./d = \frac{(C9)}{(B8)} \qquad (C10)$$

APPENDIX D

TANGENT OGIVE MASS MOMENT OF INERTIA

The nondimensional mass moment of inertia about the nose may be expressed as

$$\frac{I}{\sigma \pi d^5} = \int_o^f (x/d)^2(\rho/d)^2 \, d(x/d) \tag{D1}$$

where $(x/d)^2(\rho/d)^2$ may be expressed via equation B2 as

$$(x/d)^2(\rho/d)^2 = (f^2 + 1/4)^2(x/d)^2 - (x/d - f)^2(x/d)^2$$
$$- 2(f^2 - 1/4)(x/d)^2\sqrt{- (x/d)^2 + 2f(x/d) + (f^2 - 1/4)^2}$$
$$+ (f^2 - 1/4)^2(x/d)^2 \tag{D2}$$

Letting

$$A = \int_o^f (f^2 + 1/4)^2(x/d)^2 \, d(x/d)$$

$$B = \int_o^f (x/d - f)^2(x/d)^2 \, d(x/d)$$

$$C = \int_o^f 2(f^2 - 1/4)(x/d)^2\sqrt{- (x/d)^2 + 2f(x/d) + (f^2 - 1/4)^2} \, d(x/d)$$

$$D = \int_o^f (f^2 - 1/4)^2(x/d)^2 \, d(x/d)$$

Then,

$$\frac{I}{\sigma \pi d^5} = A - B - C + D \tag{D3}$$

where

$$A = \int_o^f (f^2 + 1/4)^2(x/d)^2 \, d(x/d) = 1/3 \, f^3(f^2 + 1/4)^2 \tag{D4}$$

$$B = \int_o^f (x/d - f)^2(x/d)^2 \, d(x/d) = 1/30 \, f^5 \qquad (D5)$$

$$C = \int_o^f 2(f^2 - 1/4)(x/d)^2\sqrt{- (x/d)^2 + 2f(x/d) + (f^2 - 1/4)^2}$$

$$d(x/d)$$

which, via formulas 184, 170 and 165, Pierce integral tables, may be expressed as follows

$$C = - 4/3 \, f(f^2 + 1/4)^3(f^2 - 1/4) + 5/6 \, f(f^2 - 1/4)^4$$

$$+ \left[5/4 \, f^2(f^2 - 1/4) + 1/4 \, (f^2 - 1/4)^3\right]$$

$$\left[f(f^2 - 1/4) + (f^2 + 1/4)^2 \sin^{-1} \left(\frac{f}{f^2 + 1/4}\right)\right] \qquad (D6)$$

$$D = \int_o^f (f^2 - 1/4)^2(x/d)^2 \, d(x/d) = 1/3 \, f^3(f^2 - 1/4)^2 \qquad (D7)$$

Substitution of equations D4, D5, D6 and D7 into D3 yields

$$\frac{I}{\sigma \pi d^5} = 1/3 \, f^3(f^2 + 1/4)^2 - 1/30 \, f^5 + 4/3 \, f(f^2 + 1/4)^3(f^2 - 1/4)$$

$$- 5/6 \, f(f^2 - 1/4)^4 - \left[5/4 \, f^2(f^2 - 1/4) + 1/4 \, (f^2 - 1/4)^3\right]$$

$$\left[f(f^2 - 1/4) + (f^2 + 1/4)^2 \sin^{-1} \left(\frac{f}{f^2 + 1/4}\right)\right]$$

$$+ 1/3 \, f^3(f^2 - 1/4)^2 \qquad (D8)$$

APPENDIX E

TANGENT OGIVE WETTED SURFACE AREA

The tangent ogive semi-cross section is shown, encompassed by its arc circle, as the cross hatched area in sketch (b).

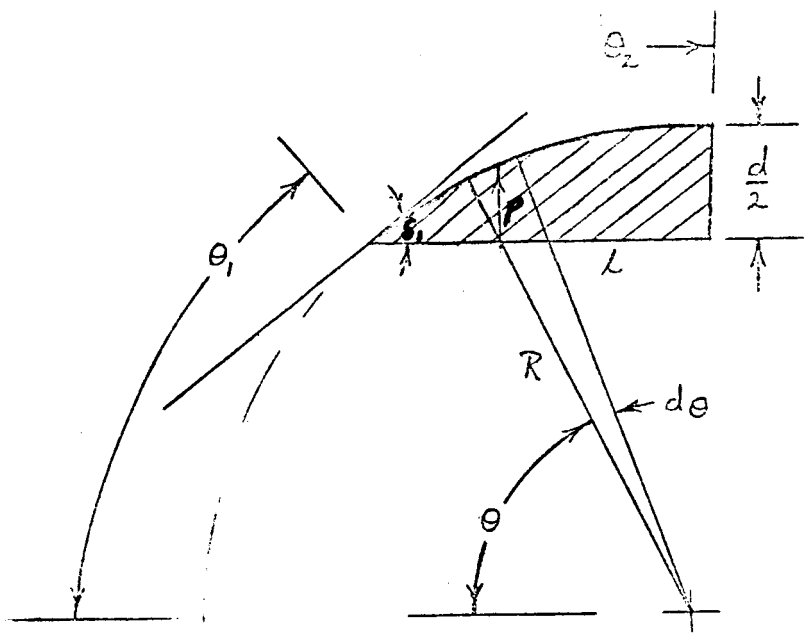

Sketch (b)

The wetted surface area is given by

$$S = 2\pi \int_{\theta_1}^{\theta_2} \rho R \, d\theta \qquad \text{(E1)}$$

Substituting

$$\rho = R \sin \theta - (R - d/2)$$

into equation (E1) and integrating ($\theta_2 = \pi/2$) yields

$$S = 2\pi R^2 \cos \theta_1 - 2\pi R(R - d/2) \left[\pi/2 - \theta_1\right]$$

Making use of the relations

$$\theta_1 = \pi/2 - \delta_1$$

$$R/d = f^2 + 1/4$$

leads to following expression for the wetted surface area

$$S = 2\pi R^2 \left\{ \sin \delta_1 - \left[1 - \frac{1}{2f^2 + 0.5} \right] \delta_1 \right\}$$

Nondimensionalizing, in terms of the base area, $S_B = \pi d^2/4$, yields

$$S/S_B = 8 \left[f^2 + 1/4 \right]^2 \left\{ \sin \delta_1 - \left[1 - \frac{1}{2f^2 + 0.5} \right] \right\}$$

δ_1 is given by equation (A7) when $x/d = \rho/d = 0$, i.e.,

$$\delta_1 = \tan^{-1} \left[\frac{f}{f^2 - 1/4} \right]$$

Hence,

$$S/S_B = 8(f^2 + 1/4)^2 \left\{ \sin \left[\tan^{-1} \left(\frac{f}{f^2 - 1/4} \right) \right] - \left(1 - \frac{1}{2f^2 + 0.5} \right) \tan^{-1} \left(\frac{f}{f^2 - 1/4} \right) \right\} \qquad \text{(E2)}$$

Flight Performance Section Files 20 September 1965

Mr. Edward E. Mayo
Flight Performance Section

CONE-CYLINDER AND OGIVE CYLINDER GEOMETRIC AND MASS CHARACTERISTICS

REFERENCE: (a) Memo of 7 July 1965, Mr. E. E. Mayo to Flight Performance Section Files, Subject: Tangent Ogive Geometric and Mass Characteristic Equations

INTRODUCTION

The nondimensionalized expressions for the geometric and mass characteristics of tangent ogives were derived in reference (a). These expressions have been evaluated and the results are presented herein. Also presented herein are characteristics for cone-cylinder and ogive-cylinder configurations. These characteristics will be utilized in nose optimization studies which are currently underway. The characteristics are presented herein to satisfy individual requests.

EQUATIONS

Nose

Ogive. - The ogive equations are obtained from reference (a) as

$$\frac{V_n}{\pi d^3} = f_n(f_n^2 + 1/4)^2 - 1/3\, f_n^3 - (f_n^2 - 1/4)(f_n^2 + 1/4)^2 \sin^{-1}\left(\frac{f_n}{f_n^2 + 1/4}\right)$$

$$(c.v./d)_n \frac{V_n}{\pi d^3} = 1/2\, f_n^2(f_n^2 + 1/4)^2 - 1/12\, f_n^4$$

$$- 2(f_n^2 - 1/4)(f_n^2 + 1/4)^2 \left[1/2\, f_n \sin^{-1}\left(\frac{f_n}{f_n^2 + 1/4}\right) - 1/3(f_n^2 + 1/4)\right]$$

$$+ 2(f_n^2 - 1/4)^2 \left[-\frac{(f_n^2 - 1/4)^2}{3} - \frac{f_n^2}{2}\right] + 1/2\, f_n^2\,(f_n^2 - 1/4)^2$$

$$\left(\frac{I_A}{\sigma\pi d^5}\right)_n = 1/3\ f_n^3(f_n^2 + 1/4)^2 - 1/30\ f_n^5 + 4/3\ f_n(f_n^2 + 1/4)^3(f_n^2 - 1/4)$$

$$- 5/6\ f_n(f_n^2 - 1/4)^4 - \left[5/4\ f_n^2(f_n^2 - 1/4) + 1/4\ (f_n^2 - 1/4)^3\right]$$

$$\left[f_n(f_n^2 - 1/4) + (f_n^2 + 1/4)^2 \sin^{-1}\left(\frac{f_n}{f_n^2 + 1/4}\right)\right]$$

$$+ 1/3\ f_n^3(f_n^2 - 1/4)^2$$

$$\left(\frac{S_W}{S}\right)_n = 8(f_n^2 + 1/4)^2 \left\{\sin\left[\tan^{-1}\left(\frac{f_n}{f_n^2 - 1/4}\right)\right] - \left(1 - \frac{1}{2f_n^2 + 0.5}\right)\right.$$

$$\left.\tan^{-1}\left(\frac{f_n}{f_n^2 - 1/4}\right)\right\}$$

Note:

The evaluation of the above expressions must be performed on the computer using double precession in order to meet accuracy requirements.

Cone. - The cone equations may be expressed as

$$\frac{V_n}{\pi d^3} = (1/12)\ f_n$$

$$(c.v./d)_n = .75\ f_n$$

$$\left(\frac{I_A}{\sigma\pi d^5}\right)_n = .05\ f_n(1/16 + f_n^2)$$

$$\left(\frac{S_W}{S}\right)_n = \sqrt{1 + 4f_n^2}$$

Afterbody

The afterbody equations are:

$$\frac{V_a}{\pi d^3} = (1/4)\, f_a$$

$$\left(\frac{c.v.}{d}\right)_a = f_n + f_a/2$$

$$\frac{I_a}{\sigma \pi d^5} = 1/16\, f_a \left[0.25 + \frac{f_a^2}{3}\right]$$

Payload

The payload equations are:

$$\frac{V_p}{\pi d^3} = \frac{V_n}{\pi d^3} + \frac{V_a}{\pi d^3}$$

$$(c.v./d)_p = \frac{\frac{V_n}{\pi d^3}(c.v./d)_n + \frac{V_a}{\pi d^3}(c.v./d)_a}{V_p/\pi d^3}$$

$$\left(\frac{I}{\sigma \pi d^5}\right)_p = \left(\frac{I_A}{\sigma \pi d^5}\right)_n - \frac{V_n}{\pi d^3}\left[\left(\frac{c.v.}{d}\right)_n\right]^2 + \frac{V_n}{\pi d^3}\left[\left(\frac{c.v.}{d}\right)_p - \left(\frac{c.v.}{d}\right)_n\right]^2$$

$$+ \frac{I_a}{\sigma \pi d^5} + \frac{V_a}{\pi d^3}\left[\left(\frac{c.v.}{d}\right)_a - \left(\frac{c.v.}{d}\right)_p\right]^2$$

$$(S_W/S)_p = \left(\frac{S_W}{S}\right)_n + \left(\frac{S_W}{S}\right)_a$$

Results

The above equations have been evaluated and the results are presented in figures 1 and 2.

Edward E. Mayo

Enclosures:

Symbols
Figures 1 and 2

cc: Mr. K. R. Medrow
Mr. J. T. Lawrence
Mr. J. S. Barrowman
Mr. H. L. Galloway

EEM:skd

SYMBOLS

c.v., c. g.	center of volume, measured aft from nose apex
d	reference diameter
f	fineness ratio
I	moment of inertia
S	reference area, $\pi d^2/4$
S_w	wetted surface area

SUBSCRIPTS

A	nose apex
a	afterbody
n	nose
p	payload

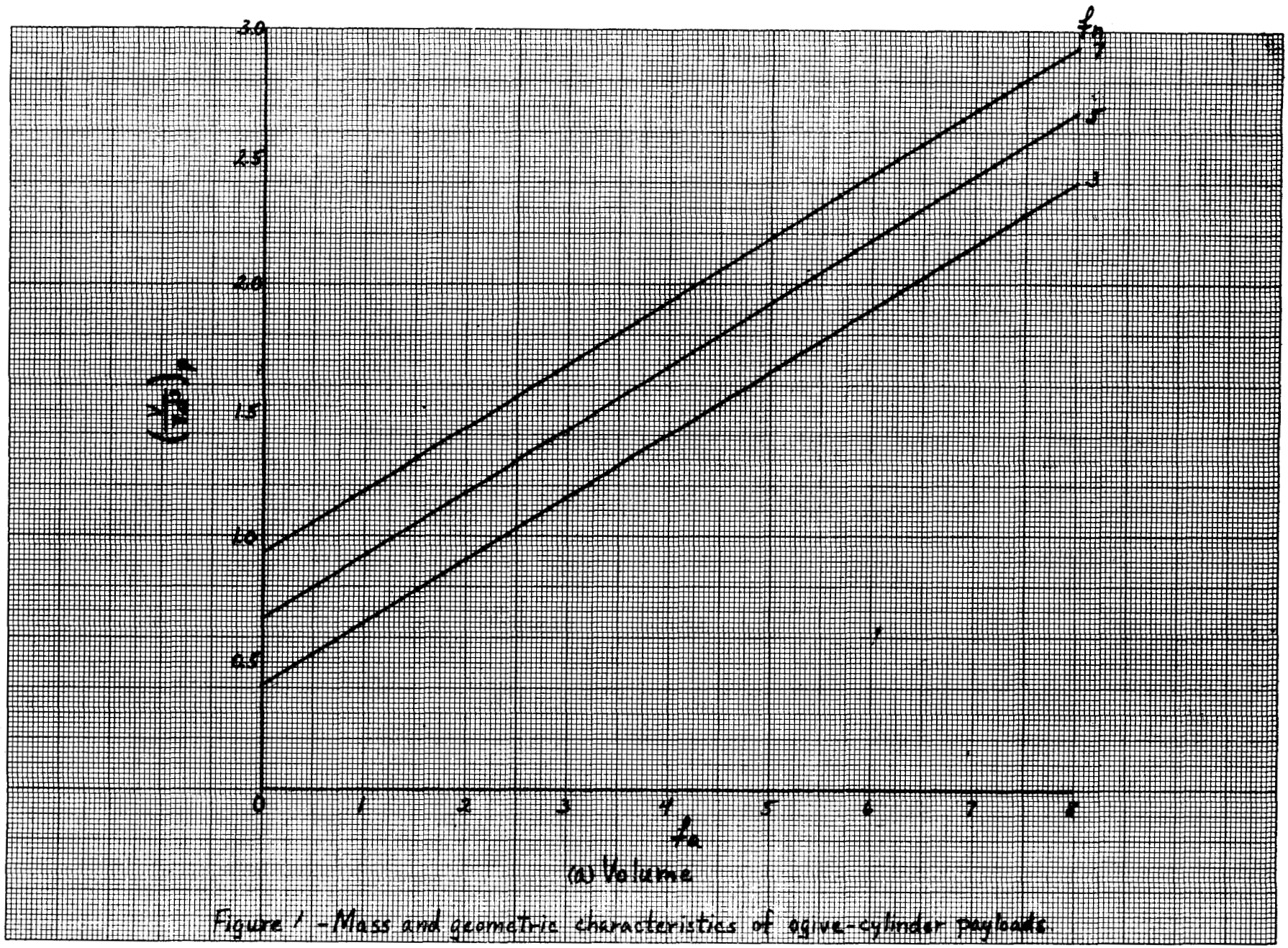

(a) Volume

Figure 1 - Mass and geometric characteristics of ogive-cylinder payloads.

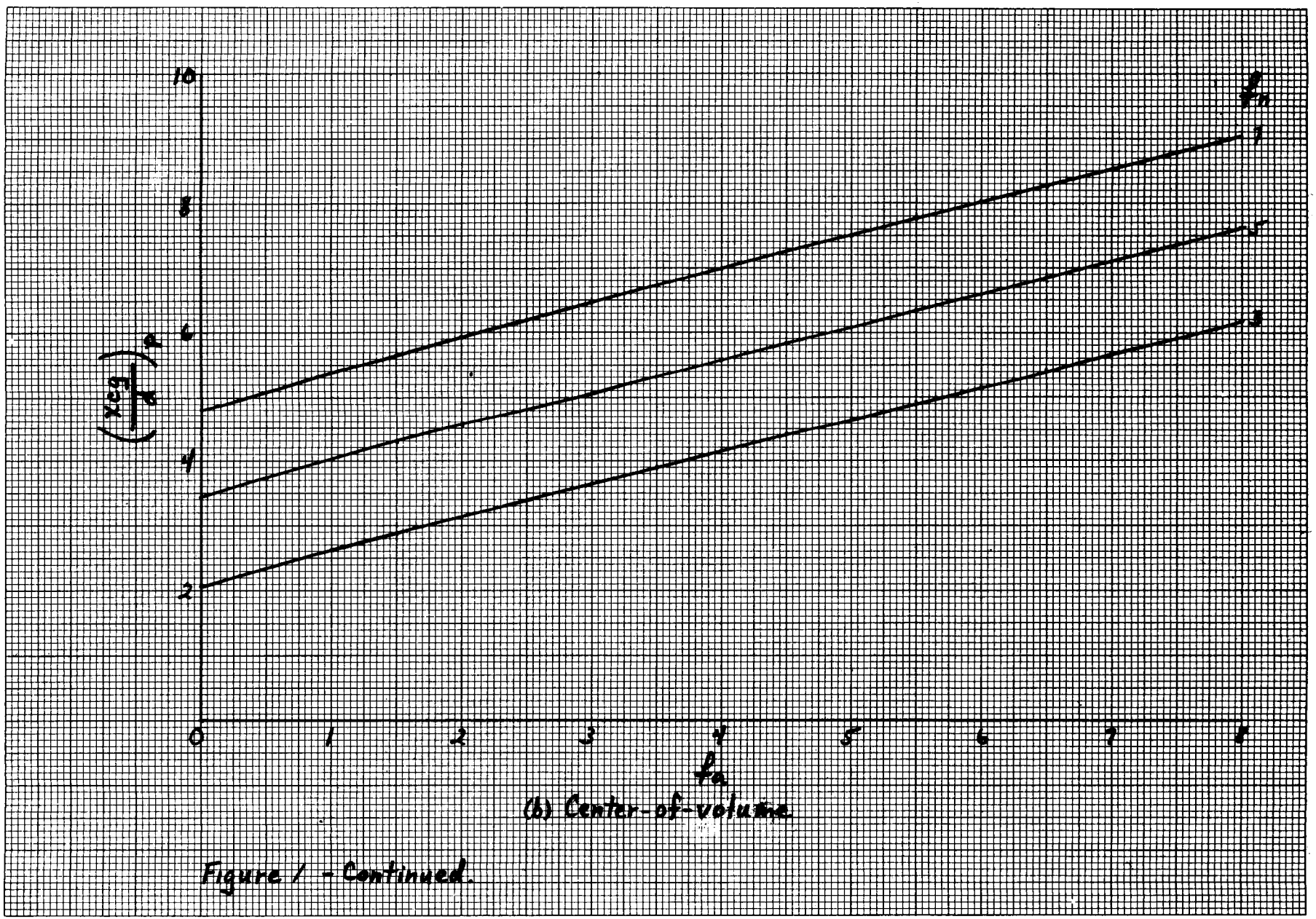

(b) Center-of-volume.

Figure 1 - Continued.

(c) Moment of inertia

Figure 1.--Continued.

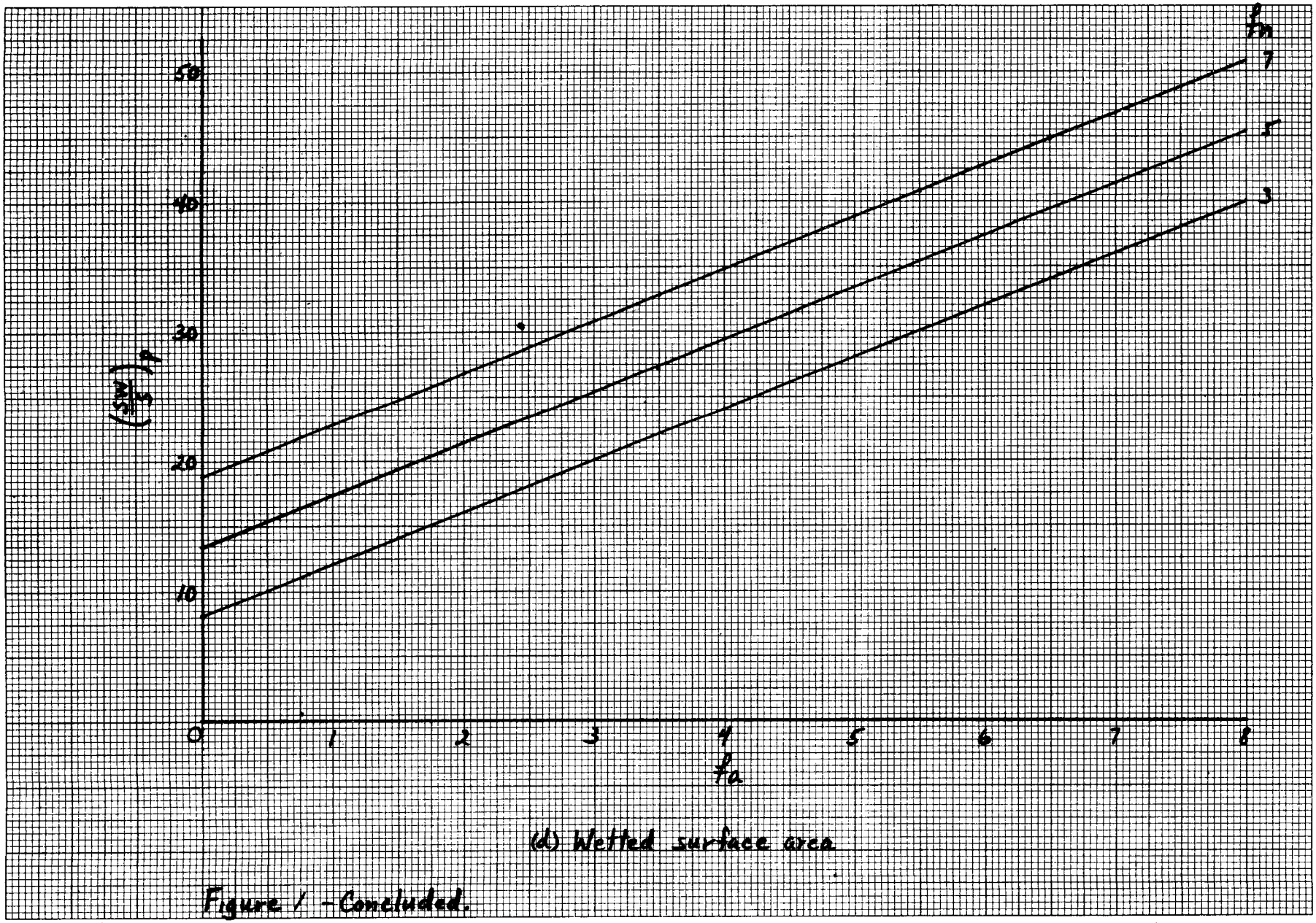

(d) Wetted surface area.

Figure 1 - Concluded.

Figure 2.- Mass and geometric characteristics of cone-cylinder payloads.

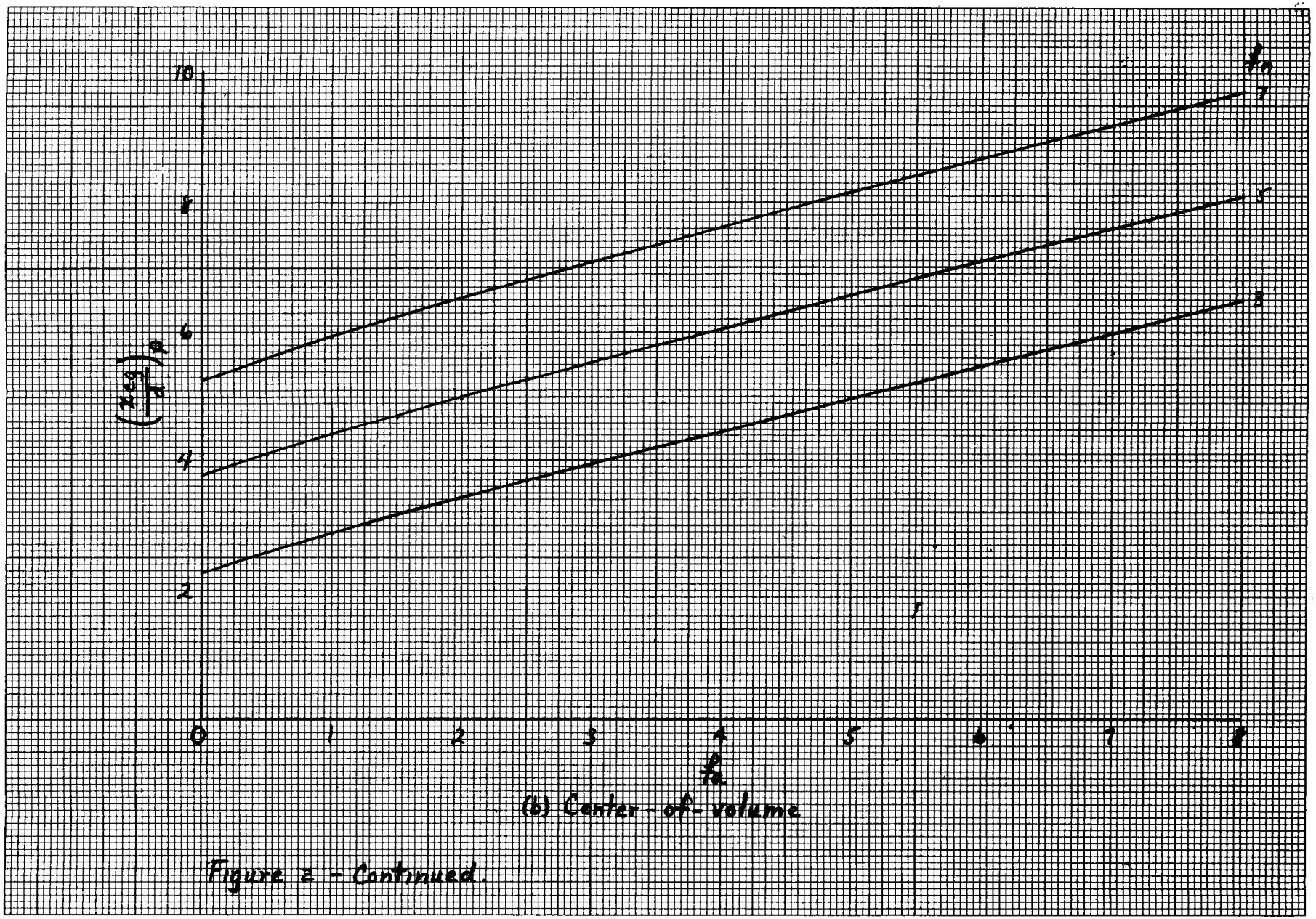

(b) Center-of-volume.

Figure 2 - Continued.

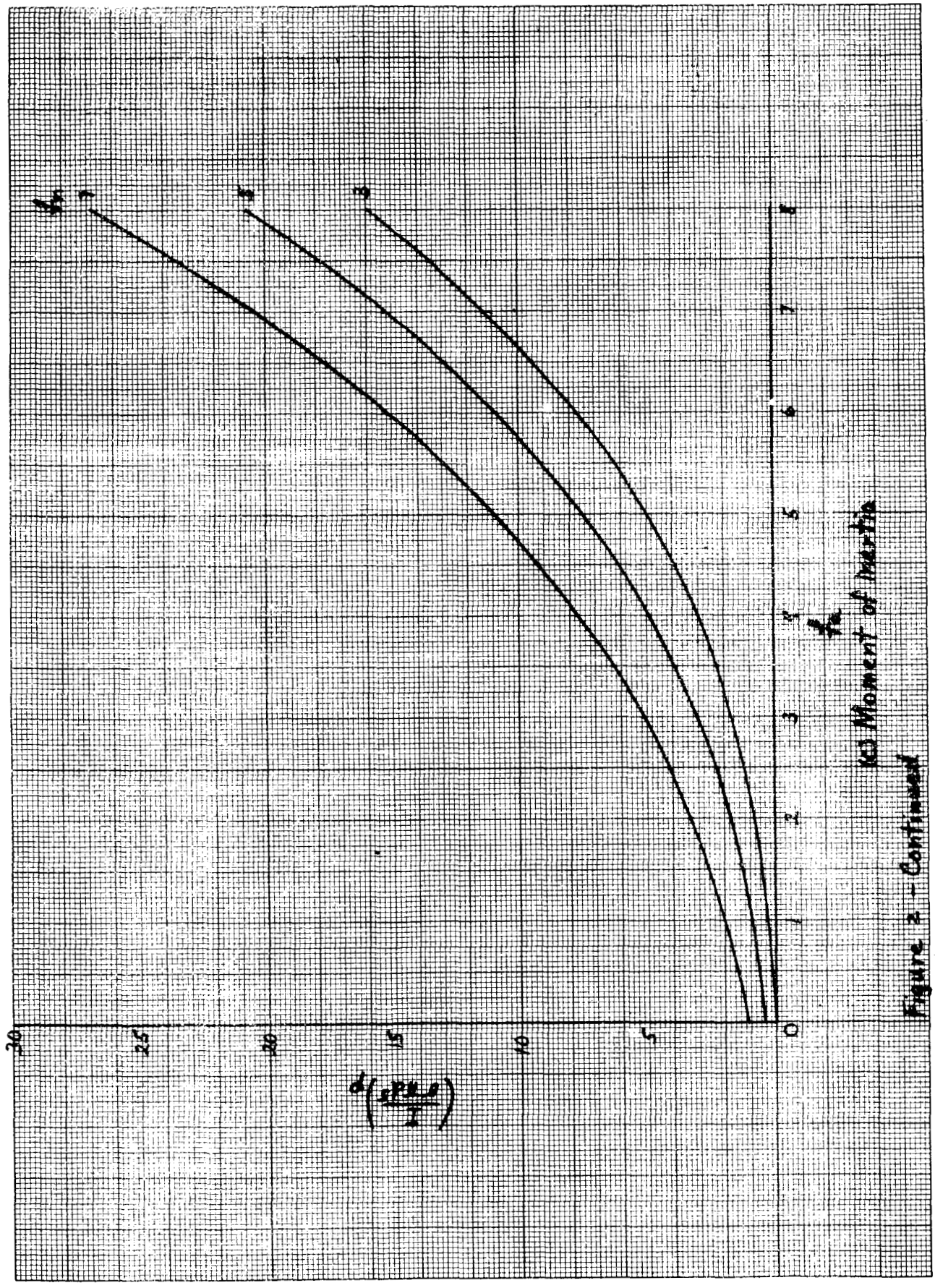
Ko Moment of Inertia
Figure 2 - Continued

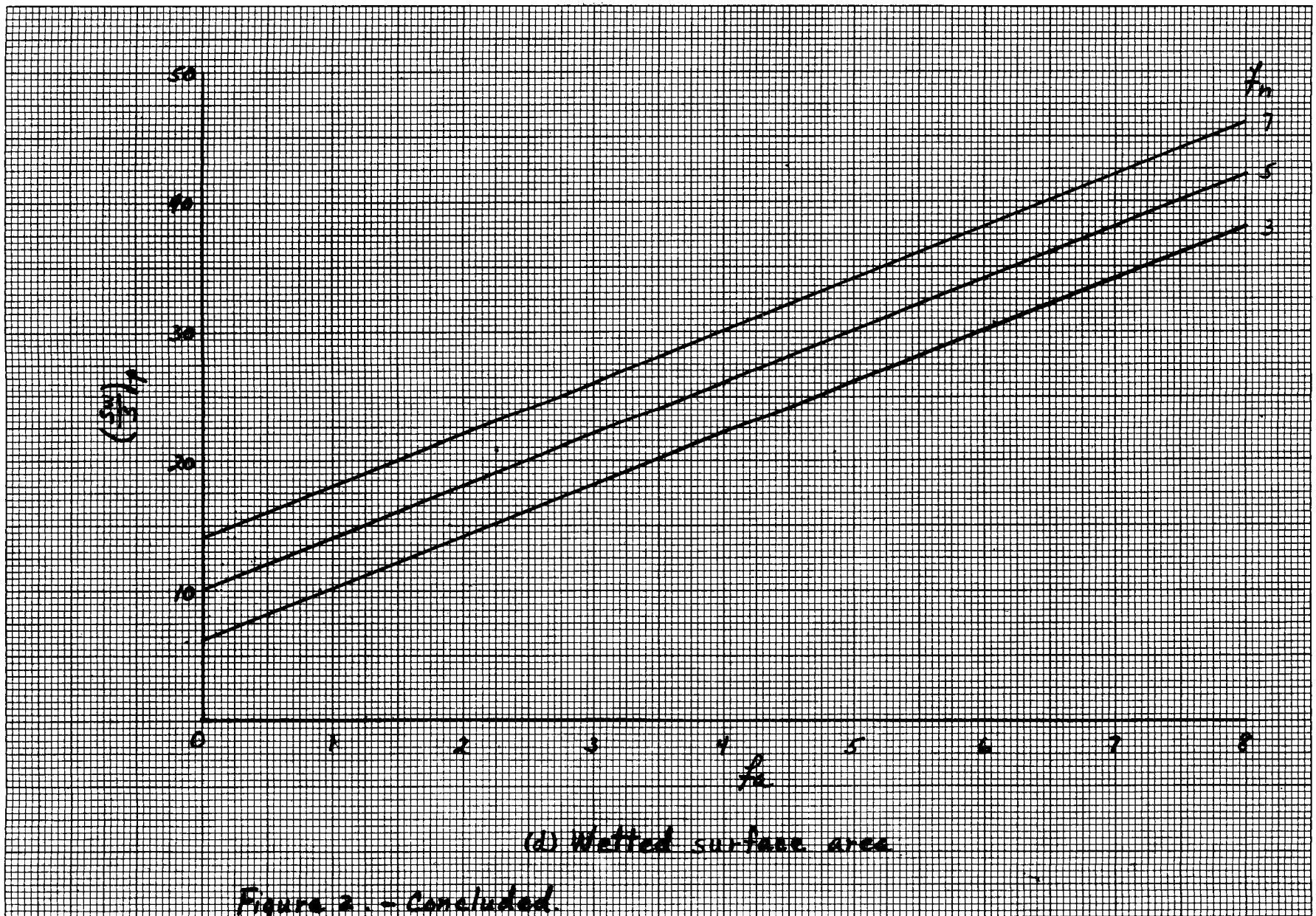

(d) Wetted surface area.

Figure 2.- Concluded.